Colour centres in germanosilicate glass and optical fibres

1994 J. Phys.: Condens. Matter 6 6901

(http://iopscience.iop.org/0953-8984/6/35/003)

J. Phys.: Condens. Matter 6 (1994) 6901–6936. Printed in the UK

REVIEW ARTICLE

Colour centres in germanosilicate glass and optical fibres

V B Neustruev

Fibre Optics Research Centre of General Physics Institute, Russian Academy of Sciences, 38 Vavilov Street, Moscow 117942, Russia

Received 23 March 1994

Abstract. This review presents the state of the art of the study of germanium-related colour centres in silica glass and silica-based fibres. Most attention is concentrated on the dominant colour centres such as the Ge-related oxygen-deficient centres and paramagnetic Ge(n) centres, all of them having ultraviolet absorption bands. The hypothetical models and formation mechanisms proposed so far for these colour centres are discussed in detail. The origins of the models and formation mechanisms and their weak and strong points are analysed. The origin of the less well studied Ge-related colour centres in the visible spectral range (GeH, GeX, drawing-dependent defects) is also discussed.

1. Introduction

Germanium dioxide is widely used in the fabrication of optical fibres to modify the refractive index of silica glass (v-SiO_2). The addition of GeO_2 does not contribute significantly to optical loss in the operating regions of fibre-optic communication systems of 1.3 and 1.55 μm. However, unlike v-SiO_2, the optical properties of germanosilicate glass and fibres are more sensitive to external influences and fabrication conditions. This is due to germanium-related defects.

There has been a plethora of publications on germanium-related defects, radiation resistance and photosensitivity of germanosilicate fibres. To date, a comprehensive phenomenological description of radiation resistance has been established [1]. In general terms the causes of photoinduced phenomena have been clarified [2]. Paramagnetic centres have been investigated in detail [3]. These subjects are continually covered by reviews.

Optical colour centres (CC) are less well understood. Only some of the centres have been identified, but the models proposed for these centres still require substantiation. Systematic investigation of the defects of germanosilicate glass based on computer simulation has begun only recently [4].

At present, mutually exclusive hypotheses and interpretations of experimental data coexist. Publications on the physics of defects, radiation resistance of fibres, photoinduced second-harmonic generation and formation of refractive-index gratings complement each other rather poorly and do not provide a unified explanation for all these phenomena. Over several decades, as the defects were studied, some hypotheses transformed into axioms without having received convincing proofs. The view of the properties of germanium defects has been changing essentially in the last 10–12 years. Nevertheless, some works still lean upon outdated concepts.

This paper is an attempt to scrutinize the results obtained so far in order to set forth firm, well founded points related to germanosilicate glass defects and to indicate moot points. Much attention is given to the properties of the intrinsic point defects, namely, to

0953-8984/94/356901+36$19.50

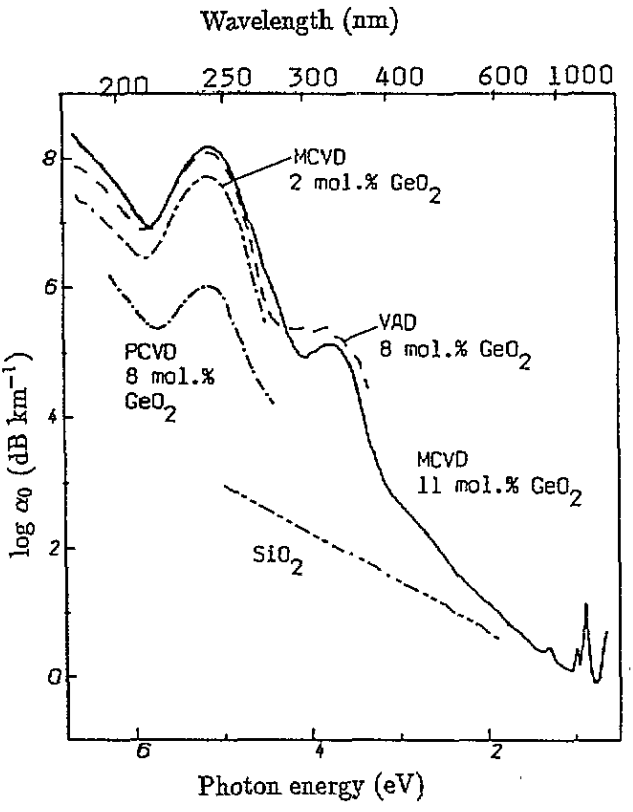

Figure 1. Initial absorption (attenuation) spectra of bulk glass samples (more than 10^4 dB km^{-1}) and fibres (less than 10^4 dB km^{-1}) [16].

the dominant CC in the initial absorption spectra of germanosilicate glass (section 2). The stable irradiation-induced CC are examined in detail (section 3), particularly the Ge-related paramagnetic centres (section 3.3).

Section 4 on the effects of hydrogen treatment is not as detailed as the importance of the subject demands. This is due to the fact that up to now empirical results prevail in the literature. However, this line of investigation is expected to provide much information about the physics of defects in future.

The subsequent sections 5 and 6 on drawing-induced defects and germanium-related radiation-induced colour centres in the visible and near-infrared regions are concerned with the origin of weakly absorbing CC, detectable only in fibres. The section titles reflect only the different modes of induction of, apparently, the same defects. Not much is so far known about the nature of these defects.

Unfortunately, it is impossible to encompass the variety of available results and conclusions in one review without making it into a bibliographic guide. That is why many interesting works are not addressed.

2. Intrinsic defects of germanosilicate glass

It follows from comparing survey absorption spectra of pure v-SiO_2 and germanosilicate glass (figure 1) that in the latter spectrum germanium-related defects prevail (see also figure 2

in which the same spectra are depicted at a linear scale). Their absorption in the ultraviolet (UV) region is 2–3 orders greater than the absorption by the v-SiO_2 intrinsic defects. The same relations are true for γ-induced absorption and for the ratio of concentrations of germanium paramagnetic centres and intrinsic paramagnetic centres of pure v-SiO_2.

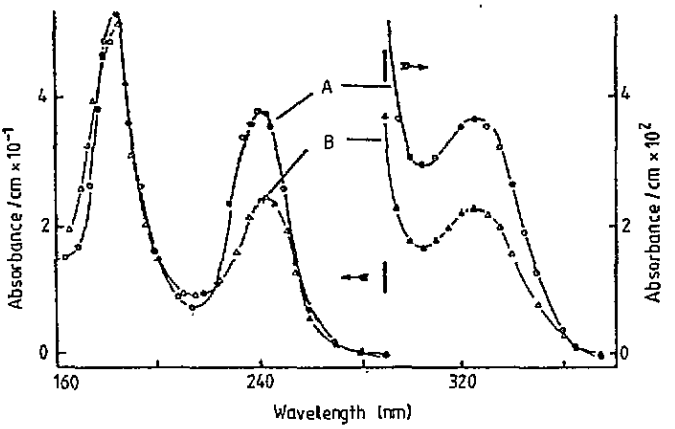

Figure 2. Absorption spectra of (A) a germanium silicate with 10.7 wt.% GeO_2 and (B) germanium phosphosilicate with 10.0 wt.% GeO_2 [8].

2.1. Germanium oxygen-deficient centres (GODC)

In germanosilicate glass an intense absorption band due to diamagnetic germanium-related defects is observed with a maximum at 242 nm (5.12 eV) along with an accompanying weak band at 330 nm (3.75 eV) [5–8]. The 5.12 eV band is a 'visiting card' of germanium in v-SiO_2. Its intensity grows in reducing conditions and with increasing glass synthesis temperature [5–8]. Under photoexcitation in the 5.12 eV band, fluorescence at 294 nm (4.22 eV) and 396 nm (3.13 eV) is observed [9–12]. There is evidence that these absorption and fluorescence bands belong to the same type of germanium-related CC [8, 9, 11, 13, 14].

There are several hypothetical models for these defects. In [5, 6, 8], the GeO molecule (in other words, Ge^{2+} centre) is considered as such a model on the basis that the defects are due to reduced germanium and their spectroscopic characteristics correlate qualitatively with the characteristics of a free GeO molecule [8].

The model of the twofold-coordinated neutral Ge atom (–O–Ge–O– or Ge_2^0 centre) [9] is apparently allied to the above model, but physically and terminologically it is more suitable to a GeO molecule bonded to the glass net. In [9] this model was strengthened by the fluorescence polarization properties, which turned out to be typical of C_{2v} symmetry defects.

The model of the antistructural defect ≡Si–Ge–Si≡ (a Ge atom substitutes a bridging oxygen) follows from the investigation of germanium diffusion in v-SiO_2, which gives rise to defects with the above properties [15].

Finally, in [10] the model of an oxygen vacancy neighbouring a Ge atom was suggested based on the analogy of the spectroscopic properties of this germanium-related defect with those of an oxygen vacancy in pure v-SiO_2. In the context of the recognized oxygen vacancy concept, this germanium-related defect shows up as a threefold-coordinated germanium atom ≡Ge...Si≡ bound to the other fragment.

All the models listed fall into the definition 'germanium oxygen-deficient centres' (GODC). Let us use this definition, as none of the models has been proved.

GODC prevail in the integral absorption by the intrinsic defects of germanosilicate glass and are precursors of the radiation-induced defects. Radiation sensitivity of fibres and photoinduced changes of optical properties are immediately associated with GODC concentration, and therefore these defects merit detailed consideration.

To my knowledge, GODC concentration was determined only in one work [6] for samples produced under typical synthesis conditions by modified chemical vapour deposition (MCVD). It turned out to be as great as 10^{-3} of the total Ge concentration in the glass. The oscillator strength in the 242 nm absorption band was determined to be $f = 0.14$. In [6] it was implied that this band was due to a single type of defect. However, later a manifestation of three types of CC with essentially different properties was noticed within this band [12, 14, 16, 17]. In terms of Gaussian resolution, to these CC correspond components with maxima at 4.75 eV (261 nm), 5.12 eV (242 nm) and 5.41 eV (229 nm) (figure 3 and table 1). Their shares in the absorption are 4, 75 and 21%, respectively.

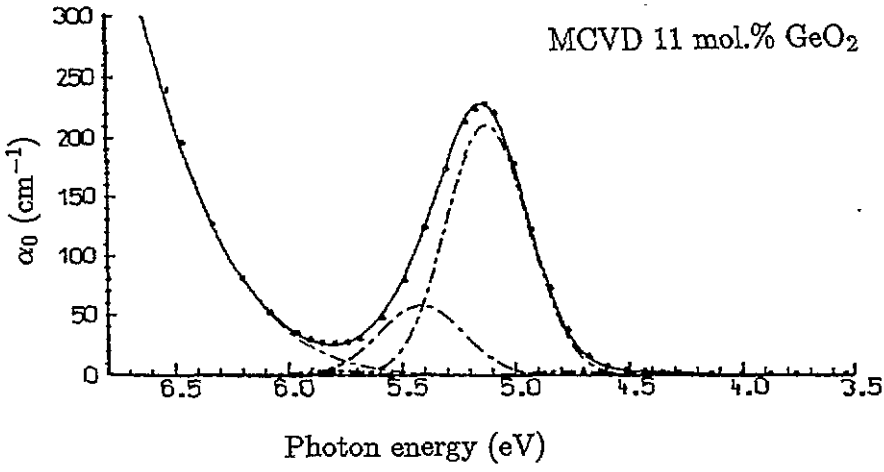

Figure 3. Initial absorption spectrum of GODC [16]: (●) experimental points; (— · —) Gaussian components; (——) their sum.

Table 1. Gaussian components of the initial 242 nm absorption band shown in figure 3.

Spectral position, E/eV (λ/nm)	4.75 (281)	5.12 (242)	5.41 (229)
FWHM (eV)	0.49	0.419	0.431
Intensity (cm^{-1})	3.3	210	57.5
Defect designation		GODC-1	GODC-2

The first component coincides with the absorption band of the non-bridging oxygen (NBO), which is an intrinsic defect of v-SiO_2, a radiation-induced CC, and is also known as a drawing-induced defect. The NBO contribution to the spectra of the initial absorption (figures 1 and 3) is negligibly small. However, on exposure to ionizing radiation, it may become comparable to or even greater than the contribution of the 4.75 eV band germanium-related CC, though the absorption of the latter defects also grows with ionizing irradiation.

The similarity of the absorption spectrum of the 4.75 eV band germanium defects and that of NBO in v-SiO_2 does not rule out the possibility of the former defects being NBO neighbouring a Ge atom (≡Ge–O˙; the dot designates an unpaired electron). However, the influence of the redox conditions on this weak absorption band of germanium defects has not been studied specially, so we restrict ourselves to stating that there exist some germanium-related defects whose absorption band overlaps strongly with the NBO absorption band in v-SiO_2.

The intense Gaussian components of 5.12 and 5.41 eV are undoubtedly GODC. Let us designate these as GODC-1 and GODC-2 respectively. The latter are radiation-induced CC (see table 4). This fact permits reliable separation of the components. It seems reasonable to attribute the concentration and f estimations in [6] to GODC-1, as these CC prevail in the absorption.

Now let us discuss the origin of the absorption band in the region $\lambda < 210$ nm, which is important for the interpretation of the mechanism of formation of radiation-induced defects. According to [8], this band peaks at 185 nm (figure 2). However, in [18] a pronounced band in this region was not observed. From the fluorescence excitation spectrum of [18] one may conclude that the maximum of the band is close to 168 nm (7.4 eV). Let us provisionally call it the 185 nm band, bearing in mind that its position should be defined more exactly.

In earlier works [6, 8, 19] this band was related to GeO_2 intrinsic absorption on the basis of indirect evidence. More recently, the 185 nm band was shown to relate to GODC [13, 20, 21]. In the reducing conditions of glass synthesis, absorption in the region $\lambda < 210$ nm grows [13, 20]. The radial distribution of absorption in preforms does not reproduce the GeO_2 distribution (see figure 6) [13]. Finally, in [20, 21] absorption suppression in the 185 and 242 nm bands was observed as a result of oxygen diffusion into the light-guiding region of a fibre.

In [20] the 185 and 242 nm bands were related to the same type of CC named germanium lone-pair centre. However the spectra presented indicate only a correlation, but not proportionality of absorption in these bands. It follows from [8] that the intensities at 185 and 242 nm do not vary in direct proportion with each other and consequently these bands are due to different germanium centres. Let us designate the centres responsible for the 185 nm absorption band as GODC-3.

2.2. *GODC luminescence*

In the absorption bands of 242 and 330 nm, luminescence is excited with a quantum yield of up to 0.65. The excitation spectra are shown in figure 4 [12]. In the 294 nm emission band the decay time is less than 10 ns; in the 396 nm emission band, 109 μs. The maxima of the emission bands vary slightly from author to author because of reabsorption.

The ratio of the absorption coefficients in the 242 and 330 nm (325 nm according to [8]) bands is constant with high accuracy in SiO_2–GeO_2 and SiO_2–GeO_2–P_2O_5 samples fabricated in different oxidizing conditions and equals 1032:1 [8]. By analogy with the free GeO molecule spectrum, the 242 nm band was attributed to the singlet-to-singlet transition $S_0 \rightarrow S_1$, and the 325 nm band to the partially forbidden singlet-to-triplet transition $S_0 \rightarrow T_1$. Conceptually the same conclusion was made in [9] with respect to the radiative transitions: $S_1 \rightarrow S_0$ (294 nm), $T_1 \rightarrow S_0$ (396 nm). Thus both pairs of bands are caused by the same type of defect, namely GODC-1. This was shown in [14] with the help of photoionization of these defects by laser radiation at 337 nm ($S_0 \rightarrow T_1$), which resulted in decay of only the GODC-1 component at 5.12 eV. Figure 5 depicts the GODC-1 energy level diagram with the transitions observed.

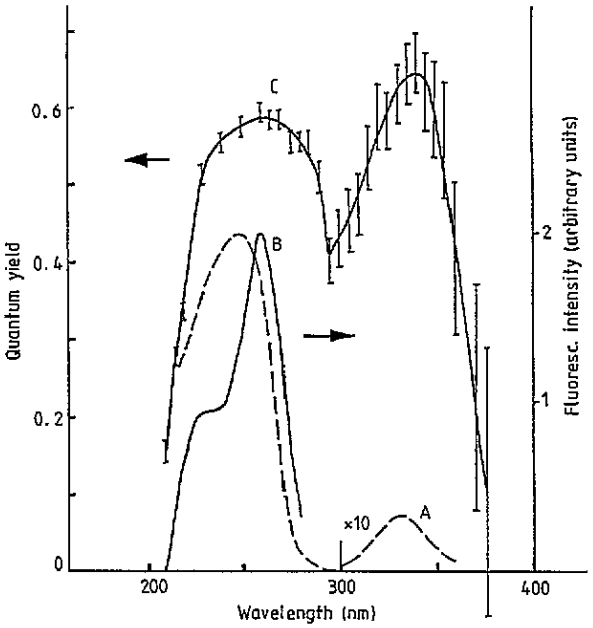

Figure 4. Excitation spectra of fluorescence at 390 nm band (A), 295 nm band (B) and quantum yield spectrum (C) at both bands [12]; 0.89 SiO_2–0.11 GeO_2 MCVD preform.

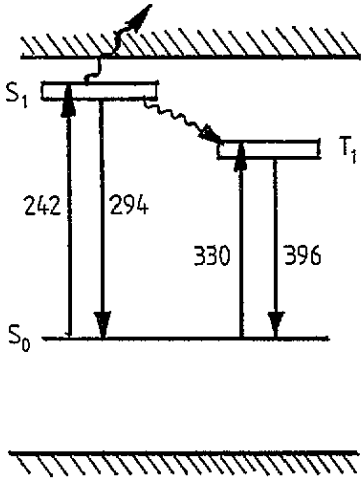

Figure 5. Energy levels of the GODC-1 and optical transitions (wavelengths in nanometres).

When exciting GODC-2 (5.41 eV), the radiative triplet-to-singlet GODC-1 transition is excited efficiently, while the $S_1 \rightarrow S_0$ transition is excited weakly or is not excited at all. The same excitation pattern was observed in [9]; however, the fall-off of the $S_1 \rightarrow S_0$ excitation in the region of 5.4 eV was supposed to be an experimental error, as the 242 nm absorption band was thought to be single-component. Interaction of GODC-1 and GODC-2 has not so far received attention.

In [22, 23], on the contrary, these peculiarities of fluorescence excitation were explained

by the existence of several fluorescence centres due to oxygen-deficient centres neighbouring Ge and Si atoms. Fluorescence spectra dependences on the excitation wavelength were investigated in germanosilicate glass samples prepared by vapour axial deposition (VAD) in different redox conditions. The slight smooth changes of the emission spectra observed in [22, 23] are obviously insufficient to draw a conclusion about the number of fluorescence centres, much less to suggest their models. It is remarkable, however, that in [23] two types of GODC were distinguished by the excitation spectra—5.17 eV (240 nm) and 4.77 eV (260 nm)—which were related to different fluorescence centres.

From the above discussion it follows that in germanosilicate glass there exist several types of diamagnetic GODC absorbing in the UV region. Unquestionably, there are correlations in the formation of these centres and, apparently, an interaction between GODC-1 and GODC-2. These points have yet to be studied. For the present, a simplified widespread concept of the GODC holds that these are oxygen vacancies with an absorption band of 242 nm.

2.3. *Formation and spatial distribution of GODC in preforms*

The formation of GODC is accounted for by the thermodynamics of the gaseous germanium redox reaction at a high synthesis temperature T:

$$GeCl_4 + O_2 \overset{T}{\rightleftharpoons} GeO_2 + 2Cl_2 \tag{1}$$

$$GeO_2 \overset{T}{\rightleftharpoons} GeO + O \tag{2}$$

With increasing temperature, reaction (2) shifts to the right, and excess chlorine in the atmosphere promotes GeO formation. This leads to the formation of oxygen-deficient centres in the glass. From thermodynamic considerations one should expect the concentrations of GeO_2 and GODC in the glass to be proportional.

There have been attempts to use the presumed proportionality of GeO_2 and GODC concentrations in order to measure GeO_2 radial distribution in preforms by absorption in the UV region [24] and by GODC fluorescence intensity [25, 26]. However, the authors of these works noticed before long that the proportionality was an exception rather than the rule. Phosphorus and boron admixtures [25], as well as treatment of preforms in H_2 atmosphere [26], strongly affected the radial distribution of fluorescence, i.e. GODC distribution. In measuring absorption, a relative increase of GODC absorption in the region of large gradients of GeO_2 concentration was regularly observed: near the core boundary and in the centre of MCVD preforms and those prepared by plasma chemical vapour deposition (PCVD) [13, 24].

Figure 6, taken from [13], depicts distributions of the three GODC types in a VAD preform jacketed by a silica tube. The GODC-1 distribution was measured through fluorescence intensity in an optically thin sample (figure 6(*a*)). The other distributions were measured through absorption at 224 nm (figure 6(*b*); GODC-2 absorption prevails) and 202 nm (figure 6(*c*); GODC-3 absorption prevails). In all cases a typical rise in the vicinity of the core boundary is seen. One can also see a disproportion between GeO_2 distribution and α(202 nm). This proves that the 185 nm band is not due to the intrinsic GeO_2 absorption. Qualitatively the same pattern was observed in standard MCVD and PCVD step-index preforms with a germanosilicate core deposited on pure silica buffer cladding.

The greatest non-uniformity of GODC was observed in PCVD step-index preforms [27]. Absorption at 242 nm revealed itself in these preforms only after collapsing, the absorption in the central region being 20 times greater than in the uniform-composition region of the

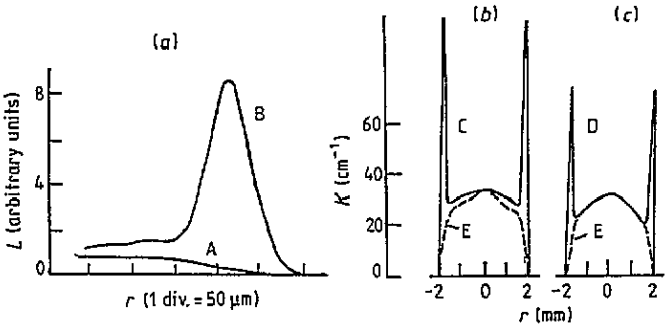

Figure 6. Radial distribution of GODC in VAD preform [13]: (*a*) fluorescence intensity in rod-in-tube samples collapsed in oxygen atmosphere (A) and hydrogen atmosphere (B) (GODC-1 distribution); (*b*) absorption coefficient at wavelength 224 nm (C) (GODC-2 dominates); (*c*) absorption coefficient α at $\lambda = 202$ nm (D) (GODC-3 dominates). Dashed lines (E) are the refractive-index profile, $\Delta n_{max} = 0.015$.

preform cross section. This peculiarity of PCVD samples was also noted in [15], where the GODC formation was found to result from GeO_2 diffusion from thin germanosilicate layers into pure silica at 1360–1700 °C.

In the PCVD process, deposition is conducted at a temperature of about 1000 °C, whereas in the MCVD process it is at 1600–1800 °C. The synthesis temperature difference leads to, approximately a 100 times difference in GODC concentration in the uniform-composition region of the preform cross section. Collapsing (about 2100 °C) affects GODC concentration in uniform regions only slightly. In preforms with graded GeO_2 distribution the disproportion between GODC and GeO_2 concentrations is less prominent.

The GODC formation is often accounted for by internal stresses. In the stressed regions, regular bonds are ruptured to produce pairs of oxygen-deficient and oxygen-redundant centres. The latter include NBO, peroxy linkage and radiation defects—peroxy radicals. This hypothesis was used to explain drawing-induced defects (NBO) in plastic-coated silica fibres [28]. Because the Ge–O bond is weaker than the Si–O bond, mainly GODC originate. Once stresses are of considerable importance, the question of complementary oxygen-redundant defects arises. To my knowledge, there have been no special investigations of the balance of oxygen-deficient and oxygen-redundant defects.

Some idea of this question can be gained from the results presented above (figures 1 and 3). In MCVD samples with 10–11 mol.% of GeO_2 the GODC concentration is about 1×10^{19} cm^{-3}. Of all oxygen-redundant centres, only NBO are optically active in the spectral region under consideration. They have two absorption bands: 4.75 eV, $\Delta(h\nu) \sim 1.05$ eV, $f \simeq 0.1$ and 2.0 eV, $\Delta(h\nu) = 0.44$ eV, $f \sim 4 \times 10^{-4}$ [29]. In the initial absorption spectrum, NBO did not reveal themselves and, judging by the absorption loss in the fibre at 2 eV, NBO concentration did not exceed 5×10^{14} cm^{-3}. It is obvious from the relation between GODC and NBO concentrations that either simultaneously with GODC a peroxy linkage is necessarily formed (inactive centre), or the mechanism of bond rupture is of little importance for the GODC formation in MCVD samples.

In this connection the diffusion mechanism of the GODC formation [15], dealing with germanium concentration gradient, deserves consideration. The authors arrive at the conclusion that GODC are formed as a result of diffusion of GeO_2 and O_2 molecules, the only possible model of GODC being the antistructural defect ≡Si–Ge–Si≡. These seemingly unexpected conclusions are based on experimental data, in contrast to the stress hypothesis. It is pertinent to note that the GODC distribution does not reproduce the stress distribution.

In MCVD samples, GODC distribution is shaped during preform fabrication and retained in a fibre in spite of additional diffusion during drawing and an increase of quenching stresses in a fibre. Recently this has been proved directly through measuring absorption spectra in preform slices and a fibre [30]. On the other hand, a strong reduction of absorption at 242 nm after drawing has been reported [31]. However, in this case optically thick fibre samples were investigated and therefore an experimental error might arise because of poor filtration of the 294 nm fluorescence band, which might give the impression of bleaching.

To sum up, the GODC formation may be attributed to three mechanisms: thermodynamic mechanism, diffusion mechanism and stress mechanism, which is less likely. In MCVD samples the thermodynamic mechanism prevails, whereas diffusion is only responsible for the disproportion of GODC and GeO_2 distributions. In PCVD samples, apparently, the diffusion mechanism is dominating; therefore one may expect the GODC concentration to increase after drawing. Nevertheless, GODC concentration in PCVD samples is less than in MCVD samples under normal conditions of preform fabrication.

2.4. GODC interaction with hydrogen, chlorine and fluorine admixtures

Much attention has been given to the investigation of these chemically active admixtures in pure v-SiO_2. In a succession of works on computer simulation of the interaction of the admixtures listed with v-SiO_2 intrinsic defects, it was shown that chlorine and fluorine atoms and molecules, interacting with all intrinsic defects and even with regular clusters, can create stable defects [32]. Unlike molecular hydrogen, the existence of fluorine and chlorine in the form of a physically dissolved gas is hardly probable.

In this section we will restrict ourselves to the evidence about the influence of these admixtures on GODC formation.

2.4.1. Hydrogen. Treatment of germanosilicate glass and fibres in hydrogen atmosphere at a high temperature increases GODC concentration. This was observed in VAD preforms sintered in hydrogen atmosphere [20, 23] (figure 7) and in MCVD preforms treated in hydrogen atmosphere at a high temperature [26].

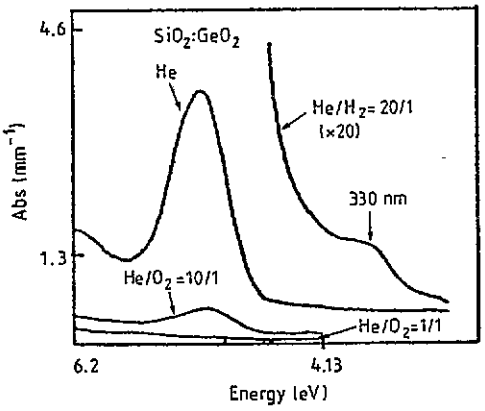

Figure 7. UV absorption spectra of 90 SiO_2–10 GeO_2 glasses sintered under different atmospheres [23].

More detailed investigations of the hydrogen treatment effect on so-called short-wavelength loss edge and defect concentration in fibres [33] showed that at a treatment

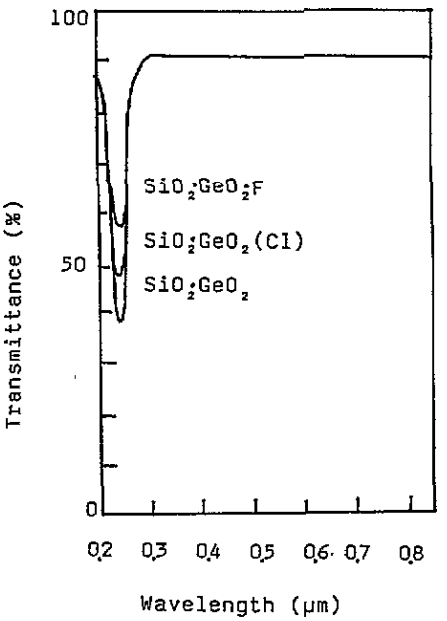

Figure 8. UV transmission spectra of unirradiated SiO_2–GeO_2 glass plates of 1.5 mm thickness. GeO_2 content with respect to $\Delta n = 1\%$, Cl content is about 1000 ppm, and F content is 1 mol.% [35].

temperature below 250 °C no changes in 242 nm band absorption occur, while at 1000 °C the absorption intensity grows strongly. According to the authors, this is due to the rupture of the regular Ge–O bonds:

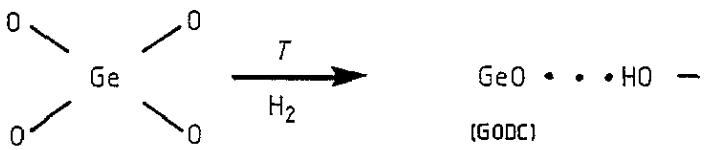

(3)

The OH group absorption and the short-wavelength loss edge grow in both cases; however, the short-wavelength loss edge spectra are a little different at different treatment temperatures.

Thus one may assume that hydrogen does not interact with GODC, but its interaction with oxygen defects such as NBO, which occurs at a high temperature, promotes GODC formation.

2.4.2. Chlorine and fluorine. Normally fibre glass contains from 0.01 to 0.1 wt.% of chlorine. Under typical synthesis conditions, the chlorine content in MCVD and PCVD samples is an order of magnitude higher than in VAD samples (provided the latter have not been chlorine-dried). However, this difference does not manifest itself in the initial fibre loss spectrum. For this reason, one may assume that chlorine does not create CC in the visible and near-infrared regions under typical conditions of germanosilicate glass synthesis.

In [34] it was noted that in VAD preforms chlorine radial distribution correlates with Ge distribution rather than with P or B. However, the data presented do not allow one to assume preferential Cl bonding to Ge.

In MCVD samples chlorine content is comparable to GODC concentration. For this reason, it seemed likely that GODC were complex germanium–chlorine defects. However, it turned out that chlorine distribution correlates with neither GODC nor Ge distributions [13]. Thus, chlorine does not enhance GODC formation; on the contrary, evidence suggests that chlorine [35] as well as fluorine [35, 36] actually suppress GODC.

Introduction of chlorine or fluorine during the sintering of VAD preforms lowered absorption at 242 nm (figure 8) and considerably improved radiation resistance of fibres in the visible and near-IR regions [35, 36]. Apparently, chlorine and fluorine, interacting with GODC, convert them into stable optically inactive centres.

3. Stable radiation-induced colour centres

On being exposed to ionizing irradiation, germanosilicate glass exhibits induced absorption, which practically reaches a steady state in an hour after irradiation at room temperature.

Many works have been devoted to stable irradiation-induced CC in bulk samples and induced absorption in fibres. These works contain a great deal of data on various aspects of defect formation. Having been obtained on different samples and in different conditions, the data and conclusions are not always in agreement. In this and subsequent sections the results of a complex investigation carried out under comparable conditions are presented [14, 16, 17, 37, 38]. One of the objectives of the investigation was to encompass as many as possible initial and radiation-induced CC in ultrahigh-purity germanosilicate glass and in fibres with germanosilicate core and pure SiO_2 cladding.

As experimental samples, preforms at various stages of preparation and fibres drawn out of these preforms were used. The best-investigated were MCVD samples. The initial reagents were additionally highly purified. The overall concentration of colouring impurities was at a level of 10^{16} cm^{-3}. Some parameters of the samples are given in table 2.

Table 2. Concentration of defects and impurities in as-prepared samples [16, 17].

Sample	Preparation technique	GeO_2 (mol.%)	Cl (cm^{-3})	OH (ppm)	Absorption at 242 nm (cm^{-1})	Ge(3) (cm^{-3})
1	MCVD	11	4.5×10^{19}	0.2	260–370[a]	3×10^{15}
2	MCVD	2	4.4×10^{19}		120	
3	VAD	8	4×10^{18}	40	300	3.1×10^{15}
4	PCVD	8	2×10^{19}		2–20[a]	5×10^{13}

[a] Variations within the cross section of the preform.

Figure 9 shows induced absorption spectra on γ-irradiation at room temperature, $\Delta\alpha = \alpha_\gamma - \alpha_0$. The initial absorption spectra of the same samples are depicted in figure 1.

Figure 10 shows induced absorption dependences, and table 3 presents relative absorption alterations α_γ/α_0 and rates of induced absorption growth $\beta \sim \log(\Delta\alpha)/\log D$. All the set of radiation-induced CC arise rather synchronously, but there are some peculiarities, among which the weak growth of induced absorption in the vicinity of 242 nm in a wide range of doses deserves particular attention. Photocoloration of these samples (section 3.1) showed that this peculiarity was connected with decay of GODC-1.

By using integral induced absorption, estimates of the lower limit of the concentration of radiation-induced CC were made for the data in figures 9 and 10. In the range from 4.2 to 6.8 eV the concentration of radiation-induced CC is not less than 7×10^{17} cm^{-3} (if $f = 1$).

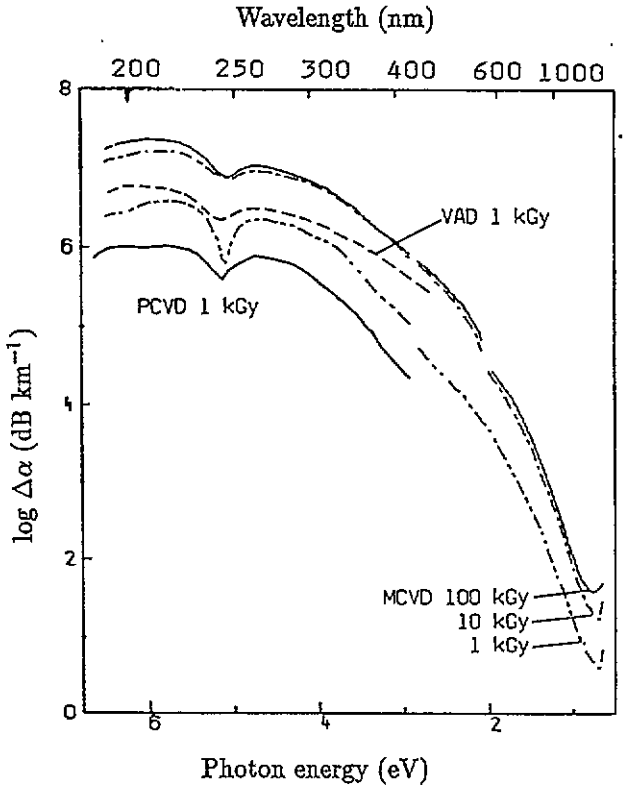

Figure 9. Gamma-induced loss spectra [16]. Initial absorption spectra of the samples are shown in figure 1.

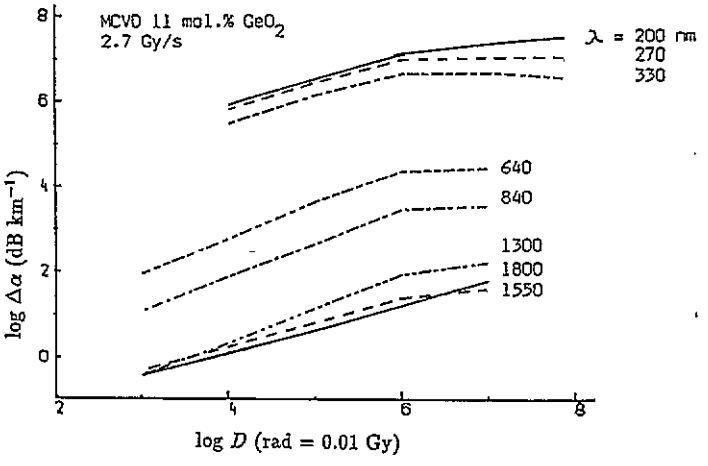

Figure 10. Dose dependence of γ-induced absorption of the samples with 11 mol.% GeO_2 as shown in figures 1 and 9 [16].

Under these irradiation conditions, the concentration of germanium-related paramagnetic centres (Ge(n) centres in terms of [39]) was as great as 8×10^{17} cm^{-3}. This means that

Table 3. Gamma-induced loss increase rates in MCVD samples with 11 mol.% GeO_2 [17].

Wavelength/nm (Photon energy/eV)	α_0 (dB km^{-1})	α_γ/α_0		β	
		10 kGy	100 kGy	0.1–10 kGy	10–1000 kGy
		Optical fibre			
1800 (0.69)	2.4	8.1	18.9	0.57	0.47
1550 (0.80)	0.83	30	48	0.53	0.2
1300 (0.96)	1.5	37	50	0.65	0.15
850 (1.46)	2.9	794	1210	0.80	0.20
800 (1.55)	3.6	1100	1510	0.80	0.14
640 (1.94)	9.5	2130	3630	0.83	0.2
600 (2.07)	13	3080	4540	0.88	0.17
		Preform			
400 (3.10)	700	1860	2140	0.65	0.1
340 (3.65)	1.1×10^5	44	35	0.7	−0.05
		Deposited layers			
270 (4.60)	1.16×10^7	2.18	2.25	0.62	0.08
242 (5.12)	1.66×10^8	1.06	1.06	—	—
212 (5.85)	1.54×10^7	2.51	3.07	0.4	0.1
200 (6.21)	5.1×10^7	1.28	1.54	0.48	0.18
190 (6.53)	1.36×10^8	1.10	1.16	0.7	0.13

residual impurities are not important for the formation of radiation-induced CC in the UV region.

From comparing the induced absorption spectra in samples fabricated by different techniques (see table 2) it follows that the chlorine impurity does not play an important part in the formation of radiation-induced CC in the UV region either. This fact does not contradict the conclusion about increased radiation resistance of fibres with chlorine. Actually, radiation sensitivity is determined by the GODC concentration: the higher the initial absorption in the 242 nm band, the higher is the radiation sensitivity, i.e. the higher is the induced absorption in all the range 190–1900 nm. Chlorine reduces GODC concentration, not forming optically active centres.

3.1. Germanosilicate glass photocoloration by UV radiation

The effect of photocoloration of germanosilicate fibres by intense argon laser radiation was noticed in [40] and used for the creation of Bragg gratings. In [41] an increase of optical loss in fibres under UV-lamp irradiation was observed. Later, paramagnetic centres and induced absorption in fibres under photoirradiation were investigated [42–45]. In [42–45], CC in the UV region were not studied.

In [16, 17] photocoloration of germanosilicate glass and fibres in a wide spectral region was examined, the samples being excited by UV lasers and a xenon flash lamp. It was established that the photocoloration occurs under excitation in the GODC absorption bands as a result of one-photon photoionization with an efficiency of up to ~ 0.1 (248 nm). The greatest efficiency was observed in the region of strong absorption by GODC-1 and GODC-3 (194 nm).

Figure 11 depicts the initial, final and induced absorption spectra on irradiation by a laser at 248 nm. Gaussian resolution of the initial and subsequent spectra revealed decay of GODC-1 and formation of radiation-induced CC (table 4). Because many conclusions have been derived from Gaussian resolution, it is necessary to describe the resolution technique.

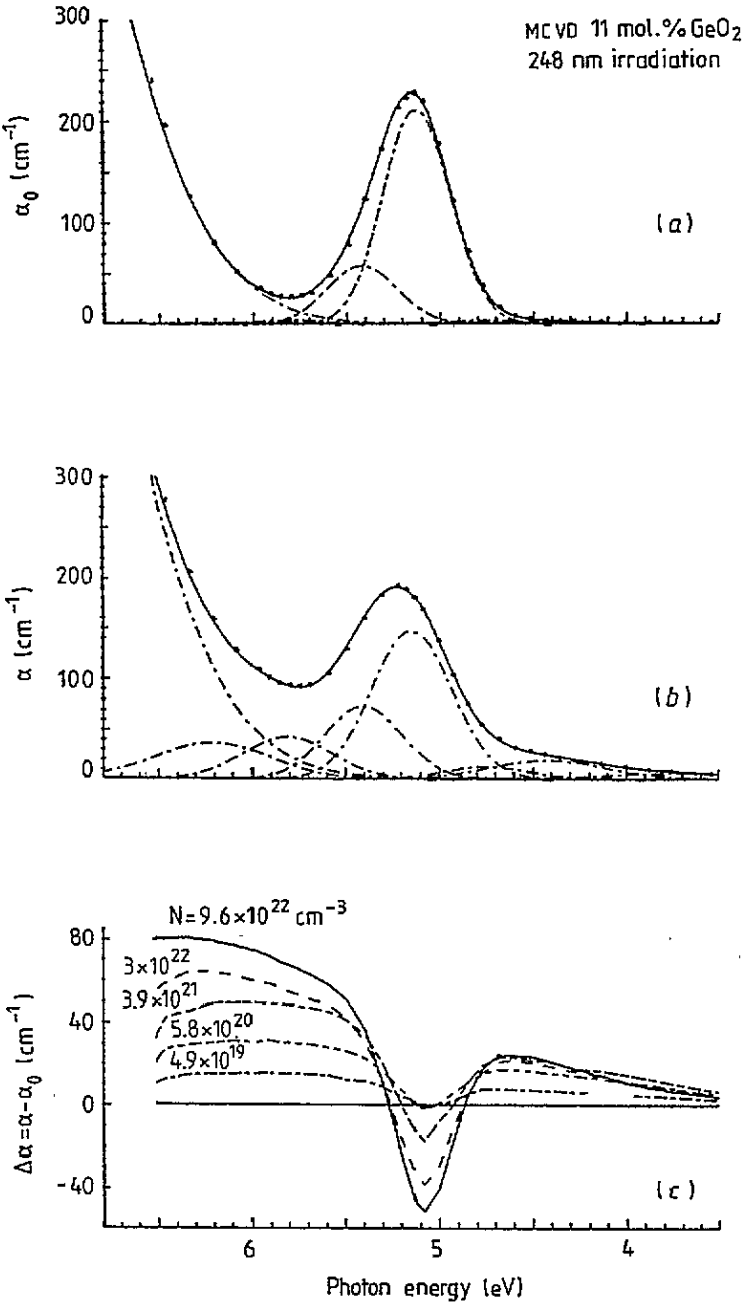

Figure 11. Initial (*a*), final (*b*) and induced (*c*) absorption spectra of Ge-doped silica glass under 248 nm irradiation [16]. In (*a*) and (*b*) the data points represent the experimental results, the broken curves represent the Gaussian components and full curves represent their sum. N is the number of absorbed photons.

The resolution was performed on measured spectra, not induced spectra, by the non-linear regression technique. The Gaussian parameters were found by iteration, the parameters being set by a random-number generator. The number of resolution components

Table 4. Parameters of Gaussian components in initial and final absorption spectra[a] after 248 nm irradiation [16].

Band position, E_i/eV (λ_i/nm)	Spectrum			
	Initial		Final[b]	
	A_i (cm^{-1})	σ_i (eV)	A_i (cm^{-1})	σ_i (eV)
3.76 (330)	—	—	5.6	0.79
4.41 (281)	1.72	0.586	18.8	0.72
4.75 (261)	3.3	0.49	12.4	0.506
5.12 (242)	210	0.419	146.8	0.50
5.41 (229)	57.5	0.431	73.7	0.48
5.81 (213)	3.98	0.433	42.5	0.55
6.2 (200)	—	—	36.2	0.72
7.5 (165)	899	1.40	1033	1.45
Standard deviation (cm^{-1})	1.86		1.12	

[a] $A = \sum A_i \exp[-(4\ln 2)(E - E_i)^2/\sigma_i^2]$.
[b] The number of absorbed photons is 9.6×10^{22} cm^{-3}.

was increased successively until achieving the minimal standard deviation from the experimental spectrum. Each spectrum was resolved independently of the others. The approximation accuracy was believed to be sufficient, if it was close to the measurement error (0.5%). For thin samples a regular error of 2 cm^{-1} was allowed. The edge absorption at $E > 6$ eV ($\lambda < 210$ nm) was approximated by one Gaussian band, whose maximum at 7.5 eV (165 nm) approximately agreed with [18] and disagreed with [8]. This component was attributed, naturally to GODC-3, but the band being outside of the measurement limits, its parameters A and σ (table 4) were not used for the estimations. Only the experimental data in proximity to the long-wavelength edge of the band were used.

The credibility of the Gaussian resolution performed is evidenced by the following facts. Independent measurements yielded the same set of components with their positions (E_i) reproduced to an accuracy of ± 0.01 eV. Spectral widths of the components (σ_i) were realistic (typical of glass). In accordance with the exposure, the behaviour of all the set of components had a simple physical meaning: gradual decay of the 5.12 eV component (i.e. GODC-1) and growth of the others, three of them being present in the initial spectrum.

A remarkable result of the resolution is a slight regular growth of σ_i of all the components with increasing exposure (at most by 0.12 eV for the 5.81 eV component). This broadening may be accounted for by Coulomb perturbation growing as charged defects accumulate. If so, this fact may be of interest in considering quantum-mechanics models of the defects.

Thus, the above results show that photodecay of GODC-1 results in increasing six types of radiation-induced CC in the UV region. In principle, one defect may have several absorption bands, but in this case the components are due to different defects, as the growth rates are different.

The 3.76 eV component in the final spectrum (figure 11, table 4) coinciding with the 330 nm singlet-to-triplet band of GODC-1 is due to a raidation-induced defect, and not GODC-1: the initial absorption in the 330 nm band of GODC-1 is 0.2 cm^{-1} and undetectable in thin samples.

After irradiation at 248 nm as well as after γ-irradiation three types of Ge(n) centres arise [39, 46].

Intense coloration and formation of three types of Ge(n) centres were also observed

under irradiation at 194 nm (6.4 eV); however, GODC-1 do not participate in this process. The 194 nm radiation falls at the edge of the GODC-3 absorption and misses the other components in the initial absorption spectrum; therefore, one may believe that the coloration occurs as a result of photoionization of GODC-3. It followed from comparing induced absorptions under irradiation at 6.4 and 5.0 eV that the radiation-induced CC with 6.2 and 5.81 eV bands are not bleached by 194 nm radiation. The fact that three types of Ge(n) centres arise under photoionization of either GODC-1 or GODC-3 has not been explained yet.

Irradiation with $E = 4.66$ eV (266 nm) produces coloration less efficiently, particularly in the region $E < 4.7$ eV. The coloration occurs due to photoionization of GODC-1. As this takes place, Ge(1) centres do not reveal themselves, being efficiently destroyed by 4.66 eV radiation [16, 17].

Irradiation with $E = 3.68$ eV (337 nm) produces very weak coloration resulting, apparently, from cascade photoionization of GODC-1 with an efficiency of $\sim 10^{-4}$ via the triplet state.

Efficient coloration is produced by non-filtered radiation of a xenon flash lamp at $\lambda > 220$ nm. In this case three types of Ge(n) centres are formed. The saturation level of the induced absorption is proportional to the radiation intensity.

The photocoloration was found to be partially reversible; nearly reversible alterations of induced absorption spectra were revealed in cyclic irradiation with photons of different energy along with a fall-off of induced absorption as pulse intensity was decreased. One may expect that this phenomenon must also take place in the case of γ-irradiation as the dose rate is decreased.

Experiments on selective photocoloration permitted more informative estimates of the radiation-induced CC concentration to be made in the assumption of the simple charge-transfer mechanism. From the data in table 4 with $f_4 = 0.14$ [6] (the index corresponds to the component number in table 4) it follows that GODC-1 were ionized to the extent of 1.0×10^{18} cm^{-3} and radiation-induced CC were formed in amounts of 2.0×10^{18} cm^{-3}, of which no less than 8.4×10^{17} cm^{-3} fell within a spectral range 3.5–6.4 eV ($f_i = 1$ for $i = 1$–7 except 4). If $f_i < 0.84$, which is more realistic, and ionized GODC-1 are optically active, then their absorption must be detectable in the region $E > 3.5$ eV too. According to which Gaussian component is due to ionized GODC-1, the upper limit of the radiation-induced CC concentration beyond the region of 3.5–6.4 eV is from 2×10^{17} to 4×10^{17} cm^{-3}. Such estimations may be used to test some hypotheses. However, below we consider facts that appear inexplicable on the basis of the simple charge-transfer mechanism.

In germanosilicate fibres, weak coloration and a photorefractive effect were observed in visible and even IR intense laser radiation. The mechanisms of these effects remain to be understood. They are assumed to be connected with multiphoton absorption falling in the 242 nm band (5 eV) [2]. However, estimations of the multiphoton absorption cross section yield excessively high values. It is pertinent to note that, for GODC-1 photoionization via the triplet state to occur, the combined photon energy of about 3.6 eV would suffice.

To sum up and to anticipate, both selective photoionization of GODC as well as γ-irradiation produce the same set of prevailing radiation-induced CC. The mode of coloration affects only the concentration ratio. Gamma irradiation does not create specific radiation-induced CC in detectable amounts. This allows us to believe that germanosilicate glass coloration is governed ultimately by charge transfer from some types of GODC, which accordingly are destroyed, to other initial defects.

3.2. Determination of the charge sign in GODC photoionization

For a long time, GODC ('oxygen vacancies') had been *a priori* assumed to be donors of

electrons. Not long ago, the charge sign was determined experimentally by the probe ion method [37].

Cerium was used as a probe ion. It enters into silica and germanosilicate glass mainly in the form of Ce^{3+} and is photoionized readily when excited in its absorption band of 320 nm, donating electrons in the process [47, 48].

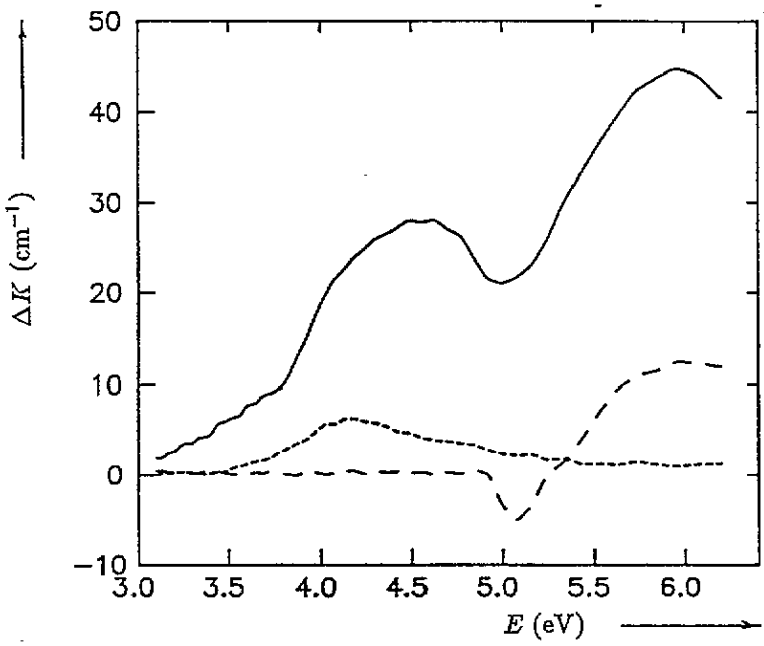

Figure 12. Induced absorption spectra after 3.68 eV irradiation [37]: (——) sample SiO_2/5 wt.% Ge/0.03 wt.% Ce, 70 J cm^{-2}; (— — —) sample SiO_2/9 wt.% Ge without Ce, 1200 J cm^{-2}; (– – –) sample SiO_2/0.06 wt.% Ce without Ge, 1200 J cm^{-2}.

Cerium in amounts of up to 0.1 wt.% was added to germanosilicate cores. At this concentration cerium does not form complex defects with germanium [49]. The efficiency of Ce^{3+} photoionization by laser radiation at 337 nm is many orders of magnitude higher than that of GODC—this fact was used to photoionize Ce^{3+} selectively.

Induced absorption (figure 12 [37]) and electron spin resonance (ESR) spectra evidenced that selective photoionization of Ce^{3+} gives rise to the same germanium-related radiation-induced CC as photoionization of GODC-1, except Ge(2) centres (see below)! This means that, being photoionized, GODC-1 donates electrons, and the resultant radiation-induced CC (except the ionized GODC-1) are electron-trapped centres. The results of [37] urge us to revise some traditional views of the mechanisms of radiation-induced CC formation, in particular regarding Ge(n) centres.

3.3. Germanium-related paramagnetic centres

Ionizing radiation induces germanium paramagnetic centres in germanosilicate glass, which resemble E′(Si) centres in v-SiO_2 [50, 51]. In [39] four types of paramagnetic centres were distinguished by distinctions in thermostability and dose dependences. These centres were supposed to have a structure similar to E′(Si) and to differ according to the number of Ge atoms ($n = 0, 1, 2, 3$) in the second coordination sphere. The centres were named Ge(n)

centres. This interpretation was based on comparison with paramagnetic centres in crystal and glass samples of GeO_2 and SiO_2 with a small content of Si and Ge, respectively.

The authors of [39] noted the mismatch between Ge(n) concentration and statistical distribution of Ge and explained it by different thermostability of the paramagnetic centres (thermostability grew with increasing n). The most stable Ge(3) centre was detectable in the glass before irradiation, and the least stable Ge(0) centre revealed itself only after high-dose irradiation, when Ge(1) and Ge(2) had been saturated. Ge(0) gave an axially symmetric signal with g-factors close to those of Ge(3). Apart from [39], Ge(0) centres were observed in [52].

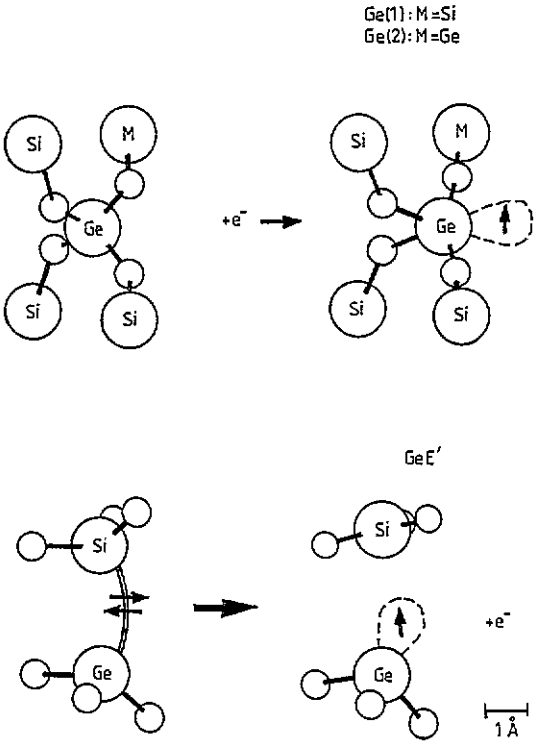

Figure 13. Models for the substitutional Ge(1,2) centres and the Ge(3) centres in irradiated Ge-doped silica. Precursor of the E′ centre is a neutral oxygen vacancy [46]. Small spheres represent oxygen atoms.

Subsequent investigations of the ESR signal hyperfine structure in samples enriched with ^{73}Ge [53, 54] revealed only two types of centres: (i) germanium electron centre (GEC) (a fourfold-coordinated Ge atom captures an electron); (ii) germanium hole centre (GeE′) (a threefold-coordinated Ge atom in the neighbourhood of an oxygen vacancy captures a hole). The latter is an analogue of the E′(Si) centre. The ESR signal of GEC corresponds to the signal of Ge(1) in [39], and that of GeE′ corresponds to Ge(3). Signals of Ge(0) and Ge(2) were not detected in [53, 54]. Moreover, the influence of Ge atoms in the second coordination sphere on the ESR signal was questioned.

In more recent works [46, 55] the authors of [39] agreed with the GEC and GeE′ models,

but strengthened the existence of Ge(2) and modified the model of Ge(2) as an electron-trapped centre, similar to Ge(1).

Although the interpretation has changed, the designation Ge(n) is now used along with GEC and GeE'. Here we will use the former designation, as the set of germanium paramagnetic centres is not limited to the two types.

Figures 13–15 show structural models, ESR signal shapes and isochronal annealing curves for Ge(n) centres.

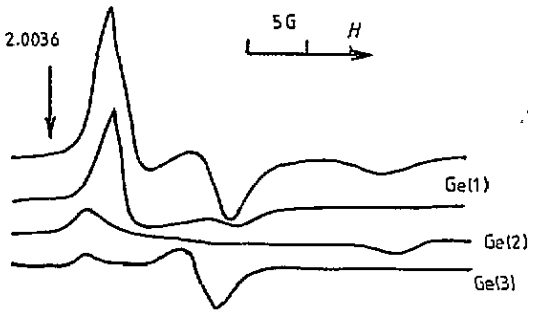

Figure 14. ESR spectrum in γ-irradiated Ge-doped silica and its components Ge(1), Ge(2) and Ge(3) resolved by isochronal annealing [17].

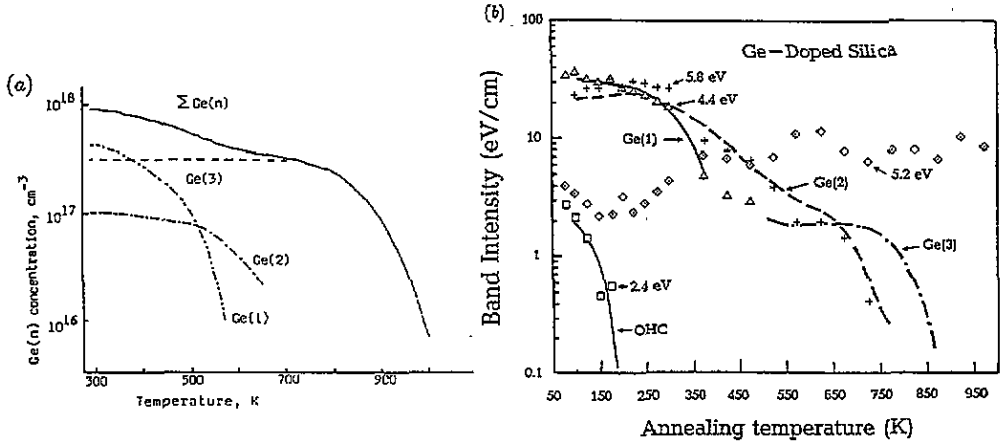

Figure 15. Isochronal annealing behaviour of Ge(n) centres: (a) 194 nm irradiation induced (number of absorbed photons 2.2×10^{23} cm^{-3}) [16]; (b) γ-irradiation induced at 77 K (full and broken curves are normalized to experimental points, which are the Gaussian band intensities [46]).

3.3.1. Other models and mechanisms of Ge(n) formation. The properties of Ge(n) centres described above are seldom subjected to question and are often invoked to explain optical properties of germanosilicate glass. However, there are facts indicative of the non-uniqueness of the models and mechanisms of Ge(n) centre formation.

By using a probe ion—a donor of electrons—it was shown that Ge(1) and Ge(3) centres are due to the precursors capturing an electron. As this takes place, Ge(2) centres not only

do not appear, but annihilate in the event that they have been previously created in the sample by, for example, γ-irradiation [37]. Thus it follows from [37] that Ge(3) may be an electron centre, but Ge(2) is a hole centre. These conclusions agree with experiment [14, 56]. According to [14], selective photobleaching of electron Ge(1) centres was attended by a decrease of the Ge(2) signal and an increase of the Ge(3) signal. In [56] an increase of the Ge(3) signal was registered under thermal annealing of Ge(1). Evidently, the models of [53, 55] do not explain these experimental facts.

The concentration of the 'electron' Ge(3) centres on prolonged exposure to laser irradiation at 337 nm was as great as 1×10^{17} cm^{-3} [37], i.e. it was typical in magnitude; therefore there are no reasons to consider them as some exotic version of Ge(3). This result does not deny the existence of hole Ge(3) centres. Moreover, in [38, 55] the existence of two types of Ge(3) centres was confirmed. Figure 16 depicts the thermal annealing curve to illustrate the presence of the two types of Ge(3) centres resulting from photocoloration [38]. Unlike figure 15, in this case the share of Ge(1) and Ge(2) was small (initially 15–20%) and was subtracted from the combined signal.

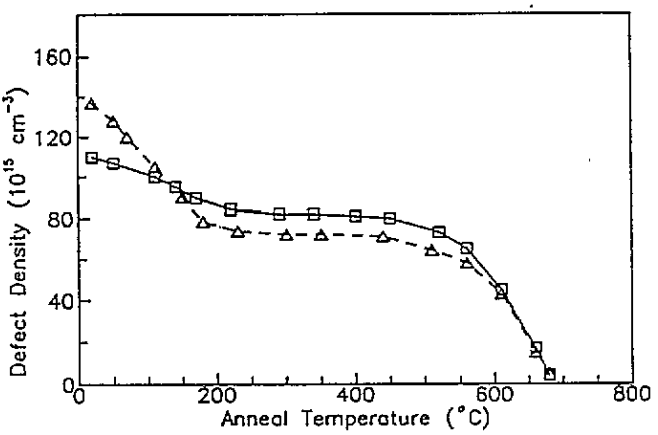

Figure 16. Isochronal annealing behaviour of Ge(3) centres, created after exposure to 4.03 eV photon, 4×10^4 J cm^{-2}, in Ge–Ce–SiO_2 (- - Δ- -) and Ge–SiO_2 (— □ —) [38].

The less stable Ge(3) centre with an annealing temperature of about 150 °C is the electron centre. By thermostability and closeness of the g-factors, the electron Ge(3) centre in [38] is similar to the Ge(0) centre in [39]. Its precursor may be a positively charged threefold-coordinated germanium atom $(Ge_3)^+$ or a doubly charged oxygen vacancy in the neighbourhood of germanium $V_O{}^{2+}$.

For completeness it should be noted that a positively charged threefold-coordinated oxygen atom $(O_3)^+$ has also been proposed as a model for Ge(3) [57].

The Ge(1) formation through capturing an electron was confirmed experimentally. The model for this centre (tetrahedron $GeO_4{}^-$) follows from considering the hyperfine structure of the ESR signal. However, it is pertinent to note that no one has observed over 10^{18} cm^{-3} Ge(1) centres in pure glass, although the precursor concentration may be as much as 10^{22} cm^{-3}. Moreover, Ge(1) centres were not detected in pure GeO_2 [55]. In this connection the computer simulation of the Ge(1) centre [4] is noteworthy. It suggests that not just any GeO_4 tetrahedron may be a precursor of a Ge(1) centre, but only that perturbed by a nearby positive charge. As an example, the model of $(GeO_4{}^-/Na^+)^0$ was computed to depict adequately the optical and paramagnetic properties of the Ge(1) centre in contrast to the

GeO_4^- defect. Obviously, the residual impurities, being deficient, cannot be the contributor of the positive charge, but radiation-induced defects can. This adequately accounts for the level of the Ge(1) concentration.

The Ge(2) centre is not, of course, a version of the Ge(1) centre. It is a hole centre and an efficient electron trap. In [58] the model of –O–Ġe = 0 was proposed for Ge(2) by analogy with the properties of formyl radical H–Ċ = 0. This model by definition corresponds to a hole centre on GODC and so does not contradict the experiment [37].

We shall now summarize the basic facts and assumptions concerning the nature of the Ge(n) centres. Ge(1) is formed on a fourfold-coordinated Ge atom through capturing an electron. For this to occur, the oxygen tetrahedron should apparently be distorted by a Coulomb field of a nearby positive charge.

There is no well founded model for the Ge(2) centre. Experiments suggest that it is a hole centre and an efficient electron trap.

The Ge(3) centres are formed on a threefold-coordinated Ge atom. There exist two types of Ge(3) distinguished by thermostability. The less stable centre arises as the result of capturing an electron. This electron Ge(3) centre resembles Ge(0) in [39]. The better-known model of Ge(3), being a hole centre that results from the donation of an electron by a threefold-coordinated Ge atom in the neighbourhood of an oxygen vacancy, has not yet received direct experimental support. Moreover, 'probe' electrons do not recombine with γ-irradiation-induced Ge(3) centres [37]. This is strange for a positively charged centre.

Because Ge(2) is formed by the donation of an electron by GODC-1 or GODC-3, one may assume that it is these initial defects that are the precursors of Ge(2). However, in this case the simple charge-transfer model will not work. First, the balance between the amount of ionized GODC and Ge(2) does not hold. Ionized centres are tens of times more numerous. Secondly, Ge(2) are not the prevailing paramagnetic centres as they should be in accordance with the simple model. The usual concentration relations at 300 K are

$$[\mathrm{Ge(1)}] > [\mathrm{Ge(3)}] > [\mathrm{Ge(2)}] \tag{4}$$

$$[\mathrm{Ge(1)}] \simeq [\mathrm{Ge(3)}] + [\mathrm{Ge(2)}]. \tag{5}$$

What has been said about Ge(2) is, for the same reasons, true for the hole Ge(3), i.e. it is not safe to say that $(\mathrm{GODC\text{-}1})^+$ or $(\mathrm{GODC\text{-}3})^+$ necessarily become Ge(3) centres.

These inconsistencies are indicative of a more complicated mechanism of GODC transformation including configurational rearrangement of $(\mathrm{GODC})^+$. The donation of an electron by GODC-1 or GODC-3 may give rise to two types of hole centres, provided there exist several stable relaxation states of $(\mathrm{GODC})^+$, or rupture and reassociation of bonds in $(\mathrm{GODC})^+$ occur in a number of ways to form either hole Ge(3) or Ge(2) centres. This is illustrated by the following diagram true for both GODC-1 and GODC-3:

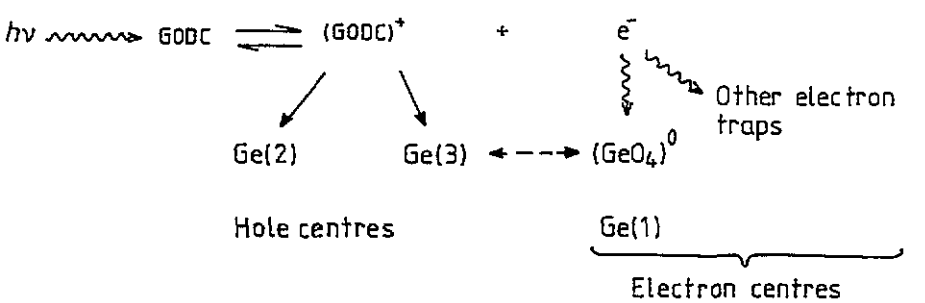

This hypothetical diagram explains the relations of concentrations (4) and (5) rather adequately, but raises a number of questions, which can be answered only with the help of numerical simulation. This diagram yields selection criteria for the models of GODC-1 and GODC-3. To anticipate, the concept of GODC-1 as a neutral oxygen vacancy in the neighbourhood of a Ge atom will not, apparently, satisfy these criteria. More suitable will be the model of an antistructural defect, if it turns out to be unstable in the positively charged state. Decay of such a defect may provide an explanation for the multitude of germanium-related radiation-induced CC.

Apart from Ge(n), in germanosilicate glass and fibres intrinsic paramagnetic centres v-SiO_2–SiE′ (OHC) are also observed, i.e. NBOHC and peroxy radicals; however, their concentration is lower than in v-SiO_2 under the same irradiation conditions. For example, Ge(3)/SiE′ ratio approximately equals 100 [39], and not 3 [54b] as one would expect.

3.3.2. Optical absorption bands of Ge(n) centres. The available data on Ge(n) absorption bands are gathered in table 5. They were obtained from comparing induced absorption spectra and ESR signals under isochronal thermal annealing of irradiated samples [46], from dose dependences and results of photobleaching of Ge(1) and Ge(2) [14, 16, 17].

Table 5. Optical absorption bands of the Ge(n) centres.

Defect	$h\nu_0$ (eV)	$\Delta h\nu$ (eV) (FWHM)	f	Ref.[a]
Ge(1) or GEC	4.4	1.97	0.42	[46]
	4.41	1.3	0.15	[14]
Ge(2)	5.8	0.9	0.77	[46]
	5.81	0.74	0.6	[14]
Ge(3) or GeE′	6.2	1.1	0.7	[14]

[a] Data from [46] and [14] obtained at a temperature of 100 K and 300 K, respectively.

In [16, 17] a strong Ge(1) photobleaching effect was revealed under excitation in their band of 4.4 eV. It was possible to identify Ge(3) centres after complete photobleaching of Ge(1) and Ge(2) by 337 nm radiation in γ-coloured samples [14]. Figure 17 shows residual induced absorption spectrum presented by the Ge(3) band of 6.2 eV on the background of absorption of diamagnetic CC. Because the Ge(3) concentration was growing during photobleaching of Ge(1) and Ge(2), the 6.2 eV band relates both to the electron Ge(3) centres and to the assumed hole Ge(3) centres induced by γ-irradiation.

In table 5 our attention is engaged by a significant discrepancy between the parameters of the Ge(1) absorption band in [14] and [46]. These parameters are essential for the interpretation of induced absorption and photosensitivity in the visible region. Therefore it should be noted that the data of [46] were obtained at 100 K. In addition, there were some difficulties with the Gaussian resolution (large errors). The data of [14] were obtained at room temperature, and the resolution errors did not exceed the measurement errors.

3.4. The analogy between γ- and photocoloration effects

The above results on the formation of stable radiation-induced CC through γ- and UV-irradiation allow us to conclude that the final result is similar rather than different. Both γ- and UV-radiations produce the same set of prevailing radiation-induced CC with

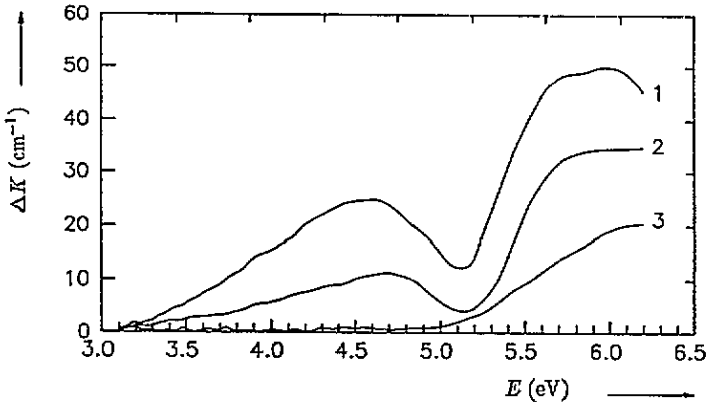

Figure 17. Induced absorption spectra of the γ-irradiated (10^4 Gy) Ge-doped silica subsequently exposed to 3.68 eV photons: (1) non-exposed, (2) 1 J cm^{-2}, (3) 100 J cm^{-2}. Ge(3) concentration rose from 1×10^{17} cm^{-3} (for curve 1) to 2×10^{17} cm^{-3} after exposure of 1.7×10^4 J cm^{-2} [14].

Table 6. Normalized ratios of induced optical absorption bands and Ge(n) concentrations [16].

Irradiation	Dose	Intensity ratio $\Delta\alpha(4.41):\Delta\alpha(5.8):\Delta\alpha(6.2)$	Concentration ratio Ge(1):Ge(2):Ge(3)
266 nm	11[a]	2.5:30:67.5	0:19:81
248 nm	1.2[a]	19:38:43	65:8:27
194 nm	22[a]	9:38:53	65:15:21
194 nm followed by 266 nm	22[a] 11[a]	4:34:61	0:20:80
Flashlamp	80 J cm^{-2}	13:31:56	67:7:26
γ (1.2 MeV)	7.4×10^5 Gy	17:36:47	56:14:30

[a] The number of absorbed photons in units 10^{22} photon/cm^3.

slightly different concentration ratios (table 6). Characteristic of both radiations is induced absorption saturation, comparable in intensity.

Certain differences might be expected in the long-wavelength region. However, the induced absorption spectra coincided ideally in the region of 400–1900 nm under some irradiation conditions (γ-irradiation: 10 kGy, 3 Gy s^{-1}; xenon lamp irradiation: 64 pulses with 62 mJ cm^{-2} per pulse) (see figure 18 [16]). This coincidence led to the conclusion that in the cited spectral region the set of electron-trapped radiation-induced CC prevails, because the hole radiation-induced CC, i.e. $(\text{GODC})^+$, must be detectable in the UV region in the case of photocoloration.

It should be noted that in [42] induced absorption spectra in fibres essentially differed after γ- and UV-irradiations (figure 19), and a conclusion was made that the final effects were quantitatively incomparable. There are a number of reasons to account for this quantitative divergence. Specifically in [42], only Ge(2) and Ge(3) centres were observed in UV-irradiated fibres. Ge(1) centres had been, evidently, photobleached by the lamp and made no contribution to the short-wavelength region in figure 19.

In [16] the relation of concentrations of Ge(n) centres after γ- and lamp irradiations was approximately the same (see table 6) with a predominance of Ge(1) centres. The fundamental similarity between the defect formation under γ- and UV-irradiations lies in

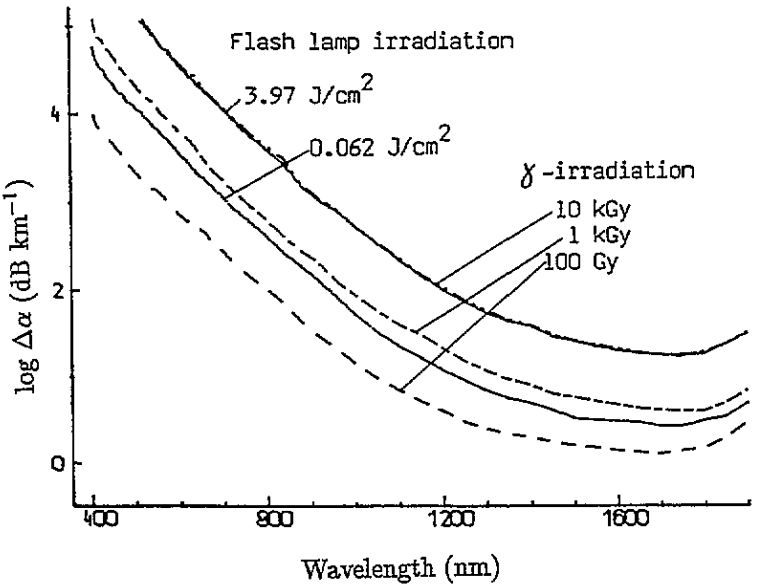

Figure 18. Induced absorption spectra of graded-index fibre (MCVD, 11 mol.% GeO_2) after γ and xenon flashlamp irradiation [16].

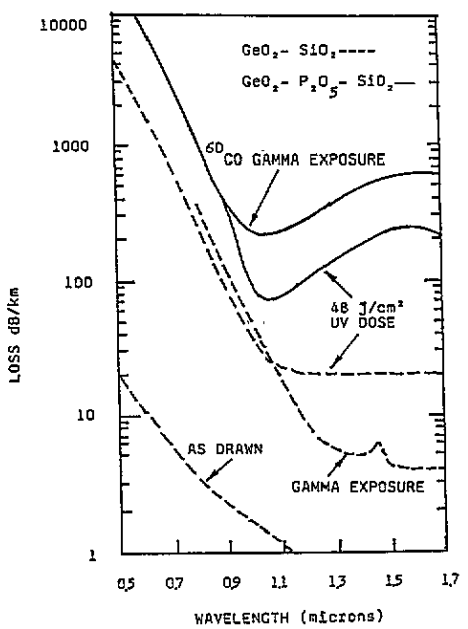

Figure 19. UV and γ radiation ($\sim 10^4$ rad) induced absorption in optical fibre [42].

the following fact. After the transient process, of the stable radiation-induced CC, those that prevail have been formed as the result of electron transfer from certain types of GODC to germanium defects (including GODC) and, apparently, to the intrinsic structural defects of glass. Gamma quanta do not create a detectable amount of peculiar radiation-induced CC

that cannot be created by UV radiation through photoionization of GODC; that is, γ-quanta do not destroy regular clusters of the glass net.

The results of [16, 17] show that the higher the GODC concentration, the poorer is the radiation resistance in a wide spectral range. Radiation resistance may be improved not only by reducing GeO_2 concentration, but by suppressing GODC too.

Recently, γ-bleaching of a photocoloured glass has been reported, which illustrates the analogy between the two processes in a new fashion [37]. The SiO_2-based sample containing 5 wt.% of Ge and 0.1 wt.% of Ce was coloured to saturation by 337 nm radiation and then γ-irradiated (10 kGy). In consequence of this, induced absorption was lowered due mainly to the recovery of Ce^{3+}. At the same time, Ge(1) and Ge(2) concentrations grew to values typical of the given γ-dose, while Ge(3) concentration turned out above the expected value, as if the normal concentration of γ-induced centres had been added to that of the photoinduced Ge(3) centres (figure 20). On the whole, the γ-bleaching had much in common with the partial reversibility of the photoinduced absorption.

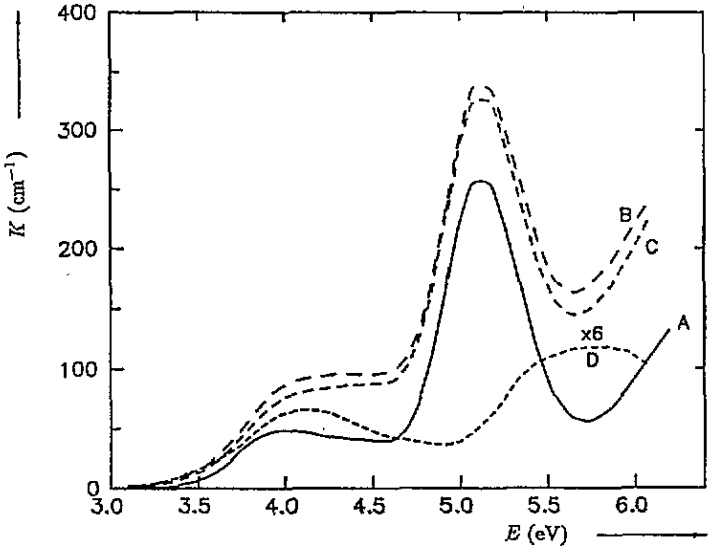

Figure 20. Absorption spectra of 0.1 wt.% Ce–5 wt.% Ge–codoped silica: (A) initial; (B) after 3.68 eV irradiation (2.1×10^4 J cm^{-2}); (C) after subsequent γ-irradiation (10^4 Gy); (D) difference between (B) and (C) [37].

4. Hydrogen treatment effects

Hydrogen readily diffuses into silica and germanosilicate glass to cause additional absorption. The absorption spectrum of dissolved molecular hydrogen is well identified. Under normal conditions, H_2 diffusion is reversible. However, in germanosilicate fibres, already at 75 °C hydrogen reactions cause irreversible additional absorption for wavelengths shorter than 1 μm [33, 59–62] (figure 21) and also a growth of the OH-group absorption bands.

In accordance with the hydrogen treatment temperature, the irreversible loss in fibres obeys the Arrhenius law. This fact is used for long-term prediction of excess loss at low

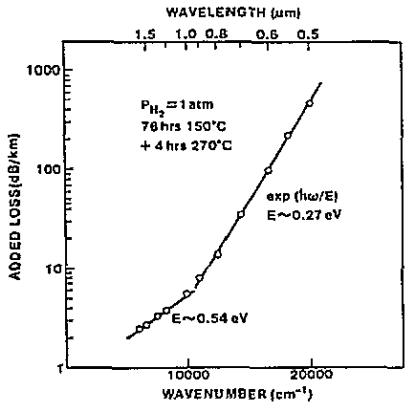

Figure 21. Short-wavelength loss edge for a conventional, GeO_2-doped core single-mode fibre [62].

temperatures [63]. OH groups are formed owing to the hydrogen interaction with glass defects [32, 59, 60, 64–66] and also with bridging oxygen [32].

Many papers have been devoted to fibre loss build-up at the 1.4 μm peak of the OH-group absorption $\Delta\alpha(1.4)$. Apart from the treatment conditions, the loss build-up rate depends on the fibre core and cladding glass composition. A number of authors [59–61, 67] noted the difficulties associated with quantitative description of the $\Delta\alpha(1.4)$ growth. This was attributed to the presence of several types of defects or to dispersion of the activation energies of the chemical reactions [59–61, 68].

The OH-group formation is most likely to occur in the vicinity of Ge and P atoms, particularly if these dopants are present at the same time [64, 66, 69–71]. This was also explained as being due to the rupture of the less strong Ge–O and P–O bonds [66], although it is known that the neighbourhood of Ge or P atoms is determined by the corresponding shift of OH absorption spectrum in Ge–OH and P–OH complexes with respect to Si–OH absorption. It is not clear why the rupture promotes Ge–OH and P–OH formation rather than Ge–H and P–H formation.

High-temperature hydrogen treatment was found to make Si–H bonds in v-SiO_2 with a fundamental frequency of 2230 cm^{-1} [63, 71]. Such a treatment of pure-silica-core fibres gave rise to a 'walking' absorption band in the vicinity of 1.5 μm [65, 66, 72], whose origin has not been established with certainty. It may be due to the second overtone of Si–H vibration (1.52 μm). However, according to [72] the band is reversible, but according to [65] it shifts up to 1.46 μm, as the absorption grows. In [59] apparently the same band with a maximum at 1.45 μm in a SiO_2/SiO_2-F single-mode fibre was related to HF absorption.

The presence of fluorine as well as phosphorus in the cladding slows down the loss growth caused by the hydrogen diffusion [66, 73–75]. Quantitative data of different authors are strongly different. In [76] it was even said that a SiO_2/SiO_2-F single-mode fibre is the least resistant to hydrogen of the other fibres containing germanium and phosphorus in the core. The ratio of hydrogen and fluorine content may account for these discrepancies. According to [77], bound fluorine readily diffuses interacting even with a bound hydrogen atom to form an HF molecule, which in turn readily diffuses too. Thus, on the one hand, fluorine slows down O–H bond making, and, on the other, hydrogen 'washes' fluorine out of the light-guiding structure, thereby degrading the light-guiding properties of fibres.

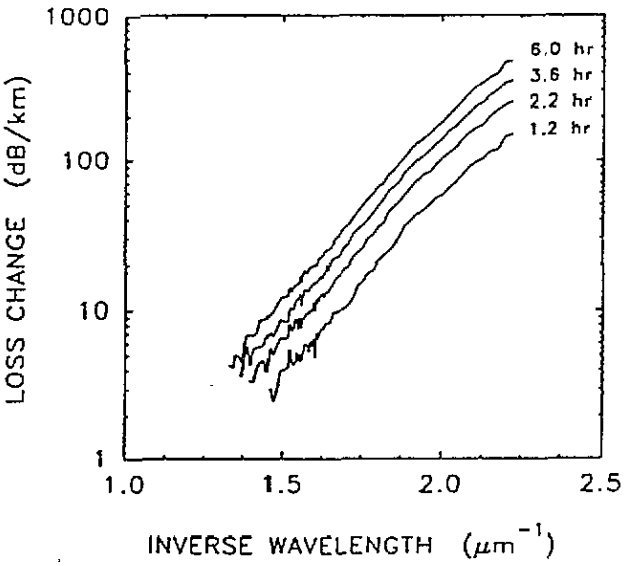

Figure 22. Hydrogen-induced loss changes at various stages of a 0.5% hydrogen treatment at 250 °C. The curves at longer times are simply shifted upwards (on a log scale), indicating an increasing concentration of a single type of defect [33].

4.1. Hydrogen-associated defects

In a number of works correlations (or anticorrelations) of induced irreversible loss with the content of known impurity-structural defects were observed. This allows one to assume that the O–H bond arises on NBO [64, 65], on drawing-induced defects with an absorption band at 630 nm [66], and also on Ge(3) centres [74]. These assumptions are based on correlations of the behaviour of colour and paramagnetic centres.

As to the origin of the short-wavelength loss edge in the region 500–950 nm, there are several hypotheses [33, 60, 61, 67], all of them asserting that the loss is due to hydrogen-associated germanium defects. These defects are sometimes called GeH defects. The latest data on the GeH centre are presented in [33]. According to this paper, different types of defects contributing to the short-wavelength loss edge appear depending on the treatment temperature. It was proposed to use the label 'GeH defects' for those defects that result from hydrogen treatment at a temperature below 250 °C. The following mechanism of GeH formation was suggested:

$$\underset{\text{Ge(3)}}{\equiv\text{Ge}^{\cdot}} \qquad {}^{\cdot}\text{O–Si}\equiv \xrightarrow[\text{H}_2]{T<250\,^{\circ}\text{C}} \underset{\text{'GeH'}}{\equiv\text{Ge–H}} \qquad \text{HO–Si}\equiv \tag{6}$$

Synchronous formation of OH groups and correlation of the short-wavelength loss edge growth with decay of Ge(3) centres count in favour of this mechanism. In a blank experiment, Ge(3) centres did not decay at the same temperature in nitrogen atmosphere. Only one type of defect ('GeH') showed up in the region 500–900 nm (figure 22), while the initial GODC did not participate in this process (the 242 nm band did not change). It is these GeH centres that have a fluorescence band of 650 nm. The authors of [33] presume Ge(3) to be the precursors of GeH only provisionally, because the ESR accuracy was insufficient to provide a quantitative proof. Recall that a different conclusion based on the correlation of Ge(3) and OH behaviour was made in [74].

High-temperature treatment (~ 1000 °C) produces a less steep slope of the short-wavelength loss edge plotted on the frequency scale and a larger absorption at 242 nm. Consequently, the short-wavelength loss edge is supposed to be caused by other mechanisms and defects initiated by rupture of regular bonds [20].

There have been several works in which hydrogen treatment was combined with ionizing irradiation [78]. To summarize these works briefly, irradiation before and after hydrogen treatment promotes hydrogen reactions peculiar to high-temperature treatment.

Another manifestation of hydrogen in germanosilicate fibres is an increase of the photorefractive effect [79, 80] and of second-harmonic generation efficiency [81, 82]. The mechanisms of these phenomena are still to be understood, although the authors point to a role of GODC [79, 80] and GeH centres [82]. Of the experimental facts, one is struck by a very significant refractive-index increase in the core of a single-mode germanosilicate fibre (by 0.02!) after the fibre has been saturated with hydrogen at high pressure and irradiated at 240 nm.

5. Drawing-induced defects

In this section defects are considered arising under non-optimal drawing regimes and contributing to excess loss in the operating spectral regions of optical communication. Defects depending on the drawing conditions (temperature, speed, tension) were noticed initially in plastic-coated silica fibres [28]. In these fibres, drawing-induced defects are recognized by a prominent absorption band around 630 nm (NBO). In germanosilicate fibres the excess loss associated with drawing conditions grows monotonically with decreasing wavelength (figure 23), similar to the short-wavelength loss edge.

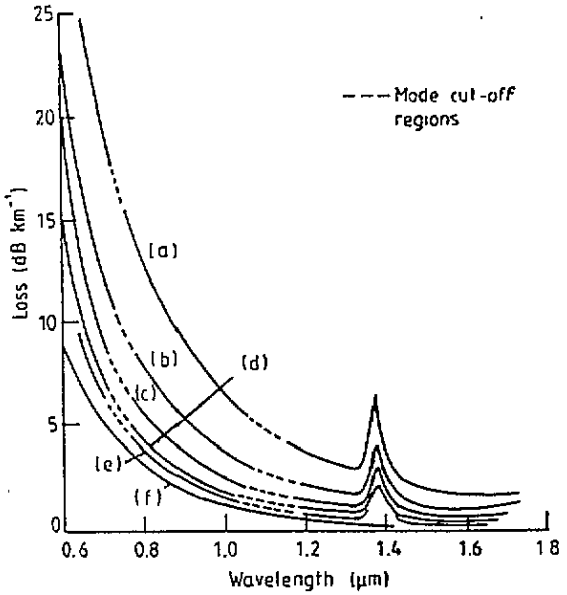

Figure 23. Dependence of losses on the fibre drawing temperature in a single-mode dispersion-shifted fibre. Temperature (°C): (a) 2150, (b) 2100, (c) 2042, (d) 1990, (e) 1940, (f) Rayleigh scattering, $\Delta n_{max} = 0.013$; (– – –) mode cut-off regions [83].

This kind of excess loss in germanosilicate fibres was investigated in detail by Ainslie *et al* [83–86]. This loss grows as the temperature is increased and the drawing speed is decreased. In addition, it depends strongly on refractive-index profile. In single-mode fibres this excess loss correlates with GeO_2 concentration, but in multimode fibres it is tens of times smaller than in single-mode ones [84, 85]. The excess loss was attributed to germanium defects arising during the drawing in the region of high thermal stresses [83]. The invoking of thermal stresses does not stand up under scrutiny.

5.1. The radiation mechanism of drawing-induced defect formation

A simple and self-consistent explanation for the drawing-induced defects was proposed in [87]. The so-called drawing-induced defects are nothing but radiation-induced defects as in the case of γ or UV irradiation. They result from GODC ionization by thermal UV radiation, which propagates from the heating zone along the silica cladding and is absorbed in the core. In accordance with their thermostability, radiation defects can arise only in a cooled fibre region. UV radiation, being absorbed in the hot region, does not produce radiation-induced CC. The concentration and assortment of defects produced depend on the exposure and spectrum of the UV radiation that has reached the cooled region. This explains the fact that the loss depends on the temperature and the drawing speed, on the temperature distribution along the fibre and on the UV radiation attenuation.

The model of [87] accounts for all the known experimental dependences of loss on drawing conditions and fibre type.

The model has been confirmed experimentally. During drawing, a fibre was additionally heated under the drawing zone to extend the length of the hot fibre region in which UV radiation is absorbed with no effect. As a result, a threefold excess loss reduction under adverse drawing conditions was demonstrated.

5.2. Formation of Ge(3) centres during preform fabrication

It is well known that radiation-induced Ge(3) defects are present in preforms and fibres that have not been irradiated. Figure 24 shows the Ge(3) concentration variation near the preform neck [88]. The Ge(3) formation is once again attributed to rupture of regular bonds in stressed regions during drawing. This explanation is acceptable for fibres, but is more than questionable in the case of preforms. The Ge(3) annealing temperature is about 700 °C, whereas in standard conditions a preform cools down from $\sim$ 2000 °C rather slowly. Despite this, as seen from figure 24, the difference of the Ge(3) concentrations in a fibre and a preform is modest.

The presence of Ge(3) centres in preforms and fibres immediately after their fabrication as well as the absence of Ge(1) and Ge(2) centres are easy to explain on the basis of the above radiation mechanism. Ge(3) centres in preforms must arise within the regions cooled down below 700 °C during the collapsing, when the hot zone temperature is $\sim$ 2000 °C. The absence of Ge(1) and Ge(2) centres means that either the preform temperature does not go below 300 °C during the collapsing or the UV radiation power is strongly weakened in the preform region with a temperature below 300 °C. Note that the measured Ge(3) concentration of 3×10^{15} cm^{-1} (see table 2) agrees well with the estimation of the concentration of the radiation-induced CC that may result from GODC photoionization by thermal UV irradiation [87].

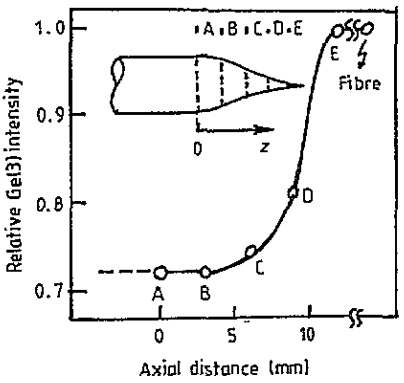

Figure 24. Ge(3) intensity spatial change in the neckdown region [88].

6. On the origin of germanium radiation-induced colour centres in visible and near-IR regions (GeX centres)

The γ and photoinduced absorption in germanosilicate fibres in the region 400–1900 nm has a minimum in the vicinity of 1500 nm, which divides this region into two parts with different dynamics of the radiation-induced CC formation. In the short-wavelength region, one sees the greatest induced absorption growth rate with saturation simultaneously with the induced absorption saturation in the UV region. The induced absorption correlates with GODC concentration. Unlike pure v-SiO_2, the induced absorption in this region is very stable. As mentioned above, electron-trapped radiation-induced CC must prevail in this region. Comparison with pure SiO_2 allows us to suppose these centres to be germanium-associated ones.

The steep monotonic induced absorption growth with decreasing wavelength gives the impression that it is the edge of an intense UV band [42]. The most suitable is the Ge(1) centre band of 4.4 eV. However, in fact this induced absorption is approximated neither by the 4.4 eV band edge nor by any other elementary band. It is an overlap of induced absorption bands of several radiation-induced CC. This is evidenced by the induced absorption growth rate dispersion (table 3) and by the different induced absorption transient kinetics on irradiation by a flash lamp (figure 25) [17]: induced absorption continues to grow in the region 640–800 nm and falls off at 400 and 1300 nm. In one hour after irradiation the absorption spectrum was practically stable; however in one year, with the fibre being kept in laboratory conditions, it changed significantly (figure 26) to disclose a new germanium CC, named GeX centre [89].

Figure 27 presents Gaussian resolution of the induced absorption in one hour after UV irradiation with 5.0 eV and in one year after γ-irradiation (curve 3 in figure 26). The GeX centre has an absorption band with maximum at 2.61 eV (475 nm) and FWHM of 0.97 eV. The following properties of the GeX centre have been revealed:

(i) GeX arises after γ-irradiation or UV irradiation with 5.0 eV, but not after powerful laser irradiation in the visible region, although induced absorption does arise in this region [2, 91]. It seems likely that GeX centres are formed under the same conditions as those that make Ge(1) formation possible.

(ii) During prolonged relaxation of excitation in laboratory conditions, the GeX concentration grows, while the Ge(1) concentration goes down, the rate of both processes being approximately equal (threefold per year as follows from optical data).

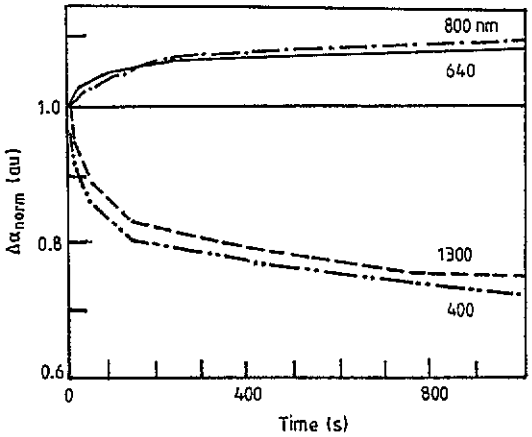

Figure 25. Induced absorption kinetics in a multimode optical fibre (MCVD, 11 mol.% GeO_2) after one pulse irradiation by xenon flash lamp [17]. Wavelengths are given in nanometres. Normalization is carried out at $t = 10$ s.

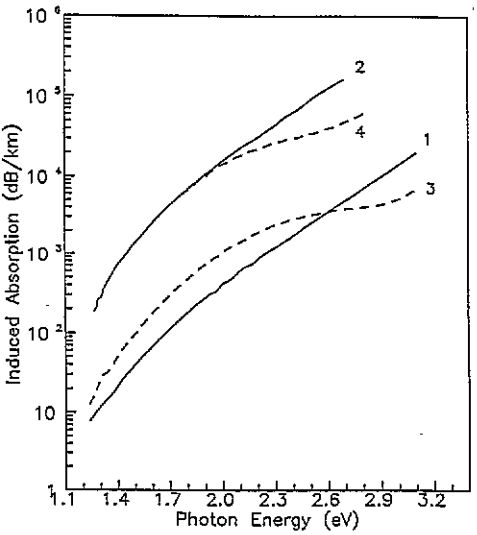

Figure 26. Induced absorption spectra of γ-irradiated fibre: (1) and (3) 100 Gy, measured 1 h and 1 year after irradiation respectively; (2) and (4) 10 kGy, 1 h and 1 year after irradiation.

(iii) At large irradiation doses the post-irradiation growth of the GeX concentration is not observed (figure 26, curves 2 and 4). Apparently, the concentration of GeX precursors is limited.

(iv) Thermo- and photostability of GeX centres is a little better than that of Ge(1). Nevertheless, both centres decay nearly synchronously under thermal annealing above 150 °C and under bleaching by green-blue laser radiation. In preliminary experiments it turned out to be impossible to accumulate GeX centres through forced destruction of Ge(1).

These experiments were carried out in the spectral region of dominating absorption of Ge(1) and GeX centres to correlate the behaviour of these centres only. The results obtained suggest that destruction of Ge(1) leads to formation of GeX. Assuming that this is due to electron transfer from Ge(1) to GeX precursors with 100% probability during post-

irradiation relaxation of excitation in laboratory conditions, one can estimate the minimal oscillator force $f \sim 1 \times 10^{-3}$ and the upper limit of GeX concentration for the data in figure 27 (see table 7). For Ge(1) and NBOHC, $f = 0.15$ and 4×10^{-4} [29] were taken.

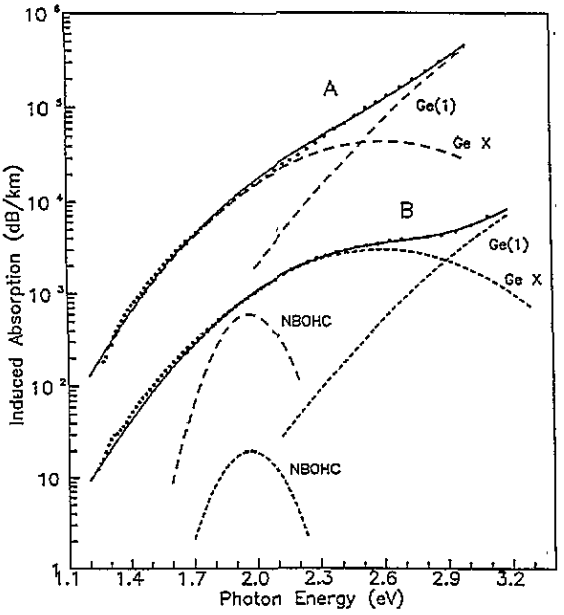

Figure 27. Gaussian simulation of induced absorption spectra: (A) 1 h after 5.0 eV photoexcitation; (B) 1 year after γ-irradiation as shown in figure 26, curve 3. The Gaussian parameters are given in table 7. Points are experimental data, broken curves are the Gaussian components, and full curves are their sum. ((A) was taken from [89]; (B) is to be published.)

Table 7. Parameters of Gaussian components simulating induced absorption spectra of irradiated fibres: $\Delta K = \sum K_i \exp[-(4\ln 2)(E - E_i)^2/W_i^2]$ where E_i = peak position of induced absorption band, K_i = peak absorption coefficient, W_i = full width at half-maximum, and N = concentration of colour centres.

Colour centre	E_i (eV)	K_i (dB km^{-1})	W_i (eV)	N (cm^{-3})	Irradiation; measurement time
Ge(1)	4.41	7.0×10^6	1.39	1×10^{18}	5.0 eV, 250 mJ cm^{-2}; 1 h after exposure
GeX	2.61	4.4×10^4	0.97	$<7 \times 10^{17}$	
NBOHC	1.97	600	0.3	7×10^{15}	
Ge(1)	4.41	2.2×10^5	1.39	3×10^{16}	γ-irradiation, 100 Gy; 1 h after exposure
GeX	2.61	1240	0.96	$<2 \times 10^{16}$	
NBOHC	1.97	30	0.3	3×10^{14}	
Ge(1)	4.41	6.3×10^4	1.37	9×10^{15}	γ-irradiation, 100 Gy; 1 year after exposure
GeX	2.61	2930	0.97	$<5 \times 10^{16}$	
NBOHC	1.97	20	0.3	2×10^{14}	

These estimations correspond to the case of strongly interacting or neighbouring defects. The model [4] for the complex Ge(1) centre $[GeO_4^-/D^+]^0$ yields just such a

pair of defects. As D^+, any closely pitched hole radiation-induced CC produced by GODC photoionization is suitable. Then electron transfer from GeO_4^- to D^+ would imply GeX formation. Unfortunately, the known hole centres are not suitable as GeX precursors from considerations of thermostability and/or the behaviour under photobleaching of Ge(1). Apparently electron transfer between the fragments of the complex Ge(1) does not give rise to GeX.

Let us consider another version. GeX results from free-electron capture by D^+:

$$\underset{\text{Ge(1)}}{[GeO_4^-/D^+]^0} + e^- \rightarrow \underset{\text{GeX or (Ge)}^-}{[GeO_4^-/D^0]^-} = [GeO_4]^- \tag{7}$$

that is, the complex Ge(1) centre itself is the GeX precursor. This version agrees with numerical simulation of the germanium substitutional in Si-site defect [4].

Negatively charged defect $[GeO_4]^-$ designated in [4] as $(Ge)^-$ is a stable paramagnetic centre with an allowed transition at 413 nm (3.0 eV) with $f \sim 0.1$ (figure 28). ESR parameters of this centre must drastically differ from those of Ge(1). Neutral fragment D^0 no longer affects $(GeO_4)^-$ properties. The latter cannot form through free-electron capture by neutral $(GeO_4)^0$ because of a potential barrier of 1.3 eV. Capture becomes likely with a nearby positive charge, but in this case the capture produces Ge(1) centre.

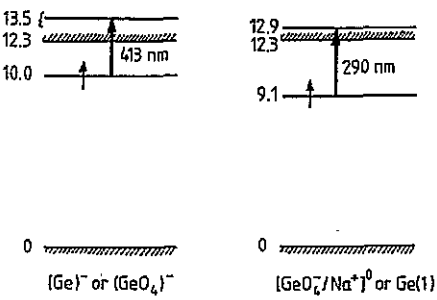

Figure 28. One-particle energy levels of (*a*) Ge substitutional in negatively charged state $(Ge)^-$ and (*b*) $[GeO_4^-/Na^+]^0$ defect. Energies in eV [4].

Taking into account the calculated value $f \sim 0.1$ for the transition of $(Ge)^-$, one obtains GeX concentration two orders lower than that given in table 7. It is possible that an ESR signal of GeX has not been detected before for this reason. Low GeX concentration may signify that electron transfer between the fragments within Ge(1) is more probable than electron detachment and its capture by another Ge(1) centre according to reaction (7). It is not improbable that GeX forms only on those Ge(1) centres whose D^+ fragment possesses certain mobility. For example, if D^+ is a self-trapped hole [90], then a thermostimulated jump of the hole must convert Ge(1) into GeX.

Thus, the last-named hypothesis concerning the origin of GeX centres agrees qualitatively with the results of numerical simulation of Ge(1) and $(Ge)^-$ defects and does not contradict the experimental facts, except one. It does not provide a simple explanation for the absence of GeX concentration growth during relaxation on exposure to large-dose irradiation. The nature of GeX centres calls for further investigation.

7. Conclusion

In this retrospective review of the investigations of the colour centres in germanosilicate glass and fibres, only the best-studied problems connected with the dominating germanium centres have been considered. The basic results and the various models for the colour centres have been discussed, arguments being advanced in favour and against. The colour centre models and formation mechanisms are still a matter for discussion. Even the models for the paramagnetic Ge(1) and Ge(3) centres, which appear to be well grounded, need refinement.

The concept of the germanosilicate glass colour centres is only beginning to emerge. Evidently, the mechanisms of the radiation defect formation are very involved. Even in the simplest case of photoionization of a single defect type, one encounters such a great diversity of defects as in the case of γ-excitation. Fortunately, in both cases, the same defects are dominating. A researcher has to look for correlations; however, when comparing two objects without regard for the other numerous participants in the unified process of defect formation, correlations may turn out to be misleading. Most reliable conclusions may derive only from investigations encompassing as many defect types as possible.

A number of important problems of defect formation call for detailed investigation. Among such problems are, first of all, identification and modelling of the initial diamagnetic colour centres, GeH and GeX centres, radiation defects remaining after high-temperature annealing. To interpret excess loss in fibres with high GeO_2 concentration, it is important to clarify the role of thermoelastic stresses and that of germanium diffusion. The elucidation of these problems will also allow us to gain insight into the micromodels of the photorefractive effect and second-harmonic generation in fibres.

Acknowledgments

The author is sincerely grateful to Professor E M Dianov for the initiation of this review and for his interest in it, to Dr A L Tomashuk who took over the translation of this paper, to Dr V M Mashinsky for his help in working on the paper, and to Ms L V Sundukova for preparation of the typescript.

This work was supported in part by AT&T Bell Laboratories.

References

[1] Friebele E J, Askins C G, Gingerich M E and Long K J 1984 *Nucl. Instrum. Methods Phys. Res. Device Appl.* B **1** 355–69

[2] Russell P St J, Poyntz-Wright L J and Hand D P 1990 *Proc. SPIE Fiber Laser Sources and Amplifiers II* vol 1373, pp 126–39

[3] Griscom D L 1991 *J. Ceram. Soc. Japan* **99** 923–42

[4] Dianov E M, Sokolov V O and Sulimov V B 1991 *Sov. Lightwave Commun.* **1** 1–27

[5] Garino Canina V 1958 *Verres et refractaires* **6** 313–23

[6] Schultz P C 1977 *Proc. 11th Int. Congr. on Glass (Prague)* vol III, pp 155–63

[7] Levy N 1981 *Appl. Opt.* **20** 460–4

[8] Yuen M J 1982 *Appl. Opt.* **21** 136–40

[9] Skuja L N, Trukhin A N and Plaudis A S 1984 *Phys. Status Solidi* a **84** K153–7

[10] Amosov A V and Petrovsky G T 1983 *Dokl. Akad. Nauk USSR* **268** 66–8 (in Russian)

[11] Trukhin A N, Boganov A G and Praulinsh A M 1979 *Fiz. Khim. Stekla* **5** 346–53 (in Russian)

[12] Guryanov A N, Gusovsky D D, Dianov E M, Mashinsky V M, Neustruev V B and Khopin V F 1982 *Dokl. Akad. Nauk USSR* **264** 90–3 (in Russian)

[13] Guryanov A N, Dianov E M, Lavrishchev S V, Mazavin S M, Mashinsky V M, Neustruev V B, Sokolov N I and Khopin V F 1986 *Fiz. Khim. Stekla* **12** 359–64 (in Russian)
[14] Anoikin E V, Guryanov A N, Gusovsky D D, Mashinsky V M, Miroshnichenko S I, Neustruev V B and Tikhomirov V A 1991 *Sov. Lightwave Commun.* **1** 29–36
[15] Rau H and Hermann W 1987 *Ber. Bunsenges. Phys. Chem.* **91** 833–40
[16] Neustruev V B, Dianov E M, Kim V M, Mashinsky V M, Romanov M V, Guryanov A N, Khopin V F and Tikhomirov V A 1989 *Fiber Integr. Opt.* **8** 143–56; 1986 *Preprint* N323, Inst. Gen. Phys., Acad. Sci. USSR, pp 1–27 (in Russian)
[17] Guryanov A N, Kim V M, Mashinsky V M, Neustruev V B, Romanov M V, Tikhomirov V A and Khopin V F 1990 *Proc. Gen. Phys. Inst. Moscow* **23** 94–113 (in Russian)
[18] Silin A R and Trukhin A N 1985 *Point Defects and Elemental Excitations in Crystalline and Vitreous SiO_2* (Riga: Zinatne) (in Russian)
[19] Cohen A J and Smith H L 1958 *J. Phys. Chem. Solids* **7** 301–6
[20] Awazu K, Kawazoe H and Yamane M 1990 *J. Appl. Phys.* **68** 2713–18
[21] Lemaire P J, Mizrahi V, Atkins R M and Kranz K S 1993 *OFC/IOOC '93 Conf. Techn. Digest* vol 4, pp 242–3
[22] Kohketsu M, Awazu K, Kawazoe H and Yamane M 1989 *Japan. J. Appl. Phys.* **28** 622–31
[23] Muta K, Kashiwazaki A and Kawazoe H 1987 *Diffus. Defect Data* **53–54** 93–8
[24] Guryanov A N, Dianov E M, Lavrishchev S V, Mashinsky V M, Neustruev V B, Nikolaichik A V and Jushin A S 1979 *Kvant. Elektron.* **6** 2109–16 (in Russian)
[25] Presby H M 1981 *Appl. Opt.* **20** 446–50 and 701–6
[26] Philen D L and Anderson W T 1982 *OFC '82 Conf. Techn. Digest* pp 66–7
[27] Kim V M 1987 *Doctoral Thesis* Gen. Phys. Inst., Moscow
[28] Kaiser P 1974 *J. Opt. Soc. Am.* **64** 475–91
[29] Skuja L N and Silin A R 1979 *Phys. Status Solidi* a **56** K11–13
[30] Atkins R M 1992 *Opt. Lett.* **17** 469–71
[31] Williams D L, Davey S T, Kashyap R, Armitage L R and Ainslie B J 1991 *Appl. Phys. Lett.* **59** 762–4
[32] Dianov E M, Sokolov V O and Sulimov V B 1990 *Proc. Gen. Phys. Inst. Moscow* **23** 122–58 (in Russian)
[33] Atkins R M and Lemaire P J 1992 *J. Appl. Phys.* **72** 344–8
[34] Hanafusa H and Tajima J 1984 *Electron. Lett.* **20** 178–9
[35] Shibata S and Nakahara M 1985 *J. Lightwave Technol.* **3** 860–3
[36] Watanabe M, Kyoto M, Yoshioka N, Kanamori H, Tanaka G, Nishimura M and Tanaka S 1984 *Proc. 10th ECOC '84 (Stuttgart)* pp 78–9
[37] Anoikin E V, Guryanov A N, Gusovsky D D, Mashinsky V M, Miroshnichenko S I, Neustruev V B, Tikhomirov V A and Zverev Yu B 1991 *Sov. Lightwave Commun.* **1** 123–31
[38] Anoikin E V, Guryanov A N, Gusovsky D D, Dianov E M, Mashinsky V M, Miroshnichenko S I, Neustruev V B, Tikhomirov V A and Zverev Yu B 1992 *Nucl. Instrum. Methods Phys. Res.* B **65** 392–6
[39] Friebele E J, Griscom D L and Siegel G H Jr 1974 *J. Appl. Phys.* **45** 3424–8
[40] Hill K O, Fujii Y, Johnson D S and Kawasaki B S 1978 *Appl. Phys. Lett.* **32** 647–9
[41] Blyler L L Jr, DiMarcello F V, Simpson J R, Sigety E A, Hart A C Jr and Foertmeyer V A 1980 *J. Non-Cryst. Solids* **38** 165–70
[42] Simpson J, Ritger J and DiMarcello F 1986 *Mater. Res. Soc. Symp.* **61** 333–8
[43] Schwartz R N, Tangonan G L, Blair G R, Chamulitrat W and Kevan L 1986 *Mater. Res. Soc. Symp.* **61** 197–204
[44] Noguchi K, Uesugi N and Suzuki K 1986 *Electron. Lett.* **22** 519–20
[45] Schwartz R N and Blair G R 1989 *J. Appl. Phys.* **65** 710–14
[46] Friebele E J and Griscom D L 1986 *Mater. Res. Soc. Symp.* **61** 319–31
[47] Stroud J S 1961 *J. Chem. Phys.* **35** 844–50
[48] Arbuzov V I, Tolstoi M N, Elerts M A and Trokshs Y S 1987 *Fiz. Khim. Stekla* **13** 581–7
[49] Anoikin E V, Guryanov A N, Dianov E M, Zverev Yu B, Mashinsky V M, Neustruev V B and Pimenov S M 1990 *Vysokochistiye Veshchestva* **1** 195–9 (in Russian)
[50] Yip K L and Fowler W B 1975 *Phys. Rev.* B **11** 2327–38
[51] Griscom D L 1985 *J. Non-Cryst. Solids* **73** 51–77
[52] Kodras G, Weeks R A and Kinser D L 1985 *J. Non-Cryst. Solids* **69** 293–8
[53] Kawazoe H 1985 *J. Non-Cryst. Solids* **71** 231–43
[54] Kawazoe H, Watanabe Y, Shibuya K and Muta K 1986a *Mater. Res. Soc. Symp. Proc.* **61** 349–57; 1986b *Japan. J. Appl. Phys.* **25** 425–31
[55] Tsai T-E, Griscom D L and Friebele E J 1987 *Diffus. Defect Data* **53–54** 469–76
[56] Hibino Y and Hanafusa H 1987 *J. Non-Cryst. Solids* **95–96** 343–50

[57] Dutta B, Kinster D L, Magruder R H III and Weeks R A 1987 *J. Non-Cryst. Solids* **95–96** 389–96
[58] Nagasawa K, Fujii T, Ohki Y and Hama Y 1988 *Japan. J. Appl. Phys.* **27** L240–3
[59] Lemaire P J and Tomita A 1984 *Proc. 10th ECOC '84 (Stuttgart)* pp 306–7
[60] Pitt N J, Marshall A, Irven J and Day S 1984 *Proc. 10th ECOC '84 (Stuttgart)* pp 308–9
[61] Wehr H and Weling F 1985 *Electron. Lett.* **21** 852–3
[62] Tomita A and Lemaire P J 1984 *Proc. 10th ECOC '84 (Stuttgart)* paper PD-1
[63] Stone J 1987 *J. Lightwave Technol.* **5** 712–33
[64] Itoh H, Ohmori Y and Nakahara M 1986 *J. Lightwave Technol.* **4** 116–20
[65] Pilon P J, Liese W and Lowe R S 1988 *Proc. OFC '88 (New Orleans) Techn. Digest* p 105
[66] Iino A, Kuwabara M and Matsuda Y 1990 *Proc. OFC '90 Techn. Digest* vol 1, p 7
[67] Uesugi N, Tokuda M, Noguchi K and Negishi Y 1984 *Proc. 10th ECOC '84 (Stuttgart)* pp 310–1
[68] Lemaire P J 1991 *Opt. Eng.* **30** 780–9
[69] Itoh H, Ohmori Y and Horiguchi M 1986 *J. Non-Cryst. Solids* **88** 83–93
[70] Rush J D, Beales K J, Cooper D M and Duncan W J 1984 *Proc. 10th ECOC '84 (Stuttgart)* pp 108–9
[71] Shelby J E 1980 *J. Appl. Phys.* **51** 2589–93
[72] Ogai M, Iino A, Matsubara K and Katsuhiko O 1986 *Proc. ECOC '86 (Barcelona)* pp 7–10
[73] Uchida N, Uesugi N, Murakami Y, Nakahara M, Tanifuji T and Inagaki N 1983 *Proc. 9th ECOC '93* paper PD-3
[74] Miyamoto M, Sanada K, Kobayashi T and Fukuda O 1985 *Proc. OFC/OFS '85 (San Diego)* pp 46–7
[75] Tamura J, Nakamura S, Kinoshita E, Iino A and Ogai M 1988 *Proc. OFC '88 (New Orleans)* p 99
[76] Anelli P, Grasso G, Modone E, Sordo B and Esposto F 1985 *Proc. IOOC/ECOC '85 (Venezia) Tech. Digest* vol 1, pp 511–14
[77] Kirchhof J, Unger S and Klein K-F 1993 *Proc. OFC/IOOC '93 (San José) Techn. Digest* vol 4, p 101
[78] Itoh H, Shimizu M, Ohmori Y and Nakahara M 1987 *J. Lightwave Technol.* **5** 134–9
[79] Meltz G and Morey W W 1991 *Proc. SPIE* **1516** 185–99
[80] Atkins R M, Mizrahi V and Lemaire P J 1993 *Proc. CLEO '93* Postdeadline Papers p 40
[81] Ouellette F, Hill K O and Johnson D C 1989 *Appl. Phys. Lett.* **54** 1086–8
[82] Krol D M, Atkins R M and Lemaire P J 1991 *Proc. SPIE* **1516** 38–46
[83] Ainslie B J, Beales K J, Day C R and Rush J D 1981 *IEEE J. Quantum Electron.* **17** 854–7
[84] Ainslie B J, Beales K J, Cooper D M, Day C R and Rush J D 1982 *J. Non-Cryst. Solids* **47** 243–6
[85] Ainslie B J, Beales K J, Cooper D M, Day C R and Rush J D 1982 *Proc. OFC '82 (Phoenix)* pp 66–7
[86] Ainslie B J, Beales K J, Cooper D M and Day C R 1983 *Proc. SPIE* **425** 15–21
[87] Belov A V, Guryanov A N, Devyatikh G G, Dianov E M, Khopin V F, Kurkov A S, Mashinsky V M, Miroshnichenko S I, Neustruev V B and Vechkanov N N 1992 *Sov. Lightwave Commun.* **2** 281–92
[88] Nakahara M, Ohmori Y, Itoh H, Shimizu M and Inagaki N 1986 *J. Lightwave Technol.* **4** 127–31
[89] Anoikin E V, Dianov E M, Mashinsky V M, Neustruev V B and Sidorin Ya S 1992 *Proc. 12th Int. Conf. Defects in Insulating Materials (Schloss Nordkirchen, Germany)* vol 2, pp 1181–3
[90] Chernov P V, Dianov E M, Karpechev V N, Kornienko L S, Morozova I O, Rybaltovskii A O, Sokolov V O and Sulimov V B 1989 *Phys. Status Solidi* b **155** 663–75
[91] Poyntz-Wright L J, Fermann M E and Russel P St J 1988 *Opt. Lett.* **13** 1023–5